Chem Soc Rev

The Chemistry of Multi-component and Hierarchical Framework Compounds

Journal:	*Chemical Society Reviews*
Manuscript ID	CS-SYN-04-2019-000250.R2
Article Type:	Review Article
Date Submitted by the Author:	17-Jun-2019
Complete List of Authors:	Feng, Liang; Texas A&M University College Station, Chemistry Wang, Kunyu; Texas A&M University, Chemistry Day, Gregory S; Department of Chemistry, Texas A&M Energy Institute, Texas A&M University, College Station, Texas Zhou, Hong-Cai; Texas A&M University, Chemistry

Journal Name

ARTICLE

The Chemistry of Multi-component and Hierarchical Framework Compounds

Received 00th January 20xx,
Accepted 00th January 20xx

DOI: 10.1039/x0xx00000x

www.rsc.org/

Liang Feng†[a], Kun-Yu Wang†[a], Gregory S. Day[a], Hong-Cai Zhou*[a, b]

Multi-component hierarchically porous materials are an emerging class of materials with tailored compositions, tunable apportionments and sophisticated applications. An increasing demand for multifunctionalities and hierarchical structures has resulted in extensive studies on multi-component hierarchical metal-organic frameworks and other open framework compounds. This review article focuses on recent advances of multi-component hierarchically porous materials, covering the design and synthetic strategies of these architectures, their characterizations, and the latest applications. Multivariate MOFs prepared under various synthetic conditions (one-pot or post-synthetic) and their building block distributions are introduced and summarized. This is followed by a short review of characterization techniques including solid-state NMR and photothermal induced resonance, and their potential applications in gas storage, separation, heterogeneous catalysis, guest delivery, and luminescence. Furthermore, guided by the same design principles, the synthesis and applications of multi-component hierarchically covalent-organic frameworks, metal-organic cages and porous organic cages are introduced and discussed. Together, this review is expected to provide a library of multi-component hierarchically porous compounds, which could also guide the state-of-art design and discovery of future porous materials with unprecedent tunability, synergism and precision.

1 Introduction

Materials science has witnessed the development and commercialization of several important classes of materials, including metal oxides, polymers, zeolites, silicons, carbons, and their composites.[1-5] These materials, mainly constructed from irreversible metallic, ionic, or covalent bonds, have been a tremendous boon, not only for the development of fundamental science, but also for the generation of new commercial and industrial products and processes. However, new and upcoming applications that focus on energy efficiency and low environmental impact require a shift in material design principles that focus on advanced tunability, precise functionality control, and synergism between structures and functionality. In particular, there is a growing interest in taking inspiration from biological systems for their ability to perform self-directed organization, replication, sorting, and correcting of both themselves and their substrates.

[a] Department of Chemistry, Texas A&M University, College Station, Texas 77843-3255.
[b] Department of Material Science and Engineering, Texas A&M University, College Station, Texas 77843-3003, United States.
† These authors contributed equally to this work.

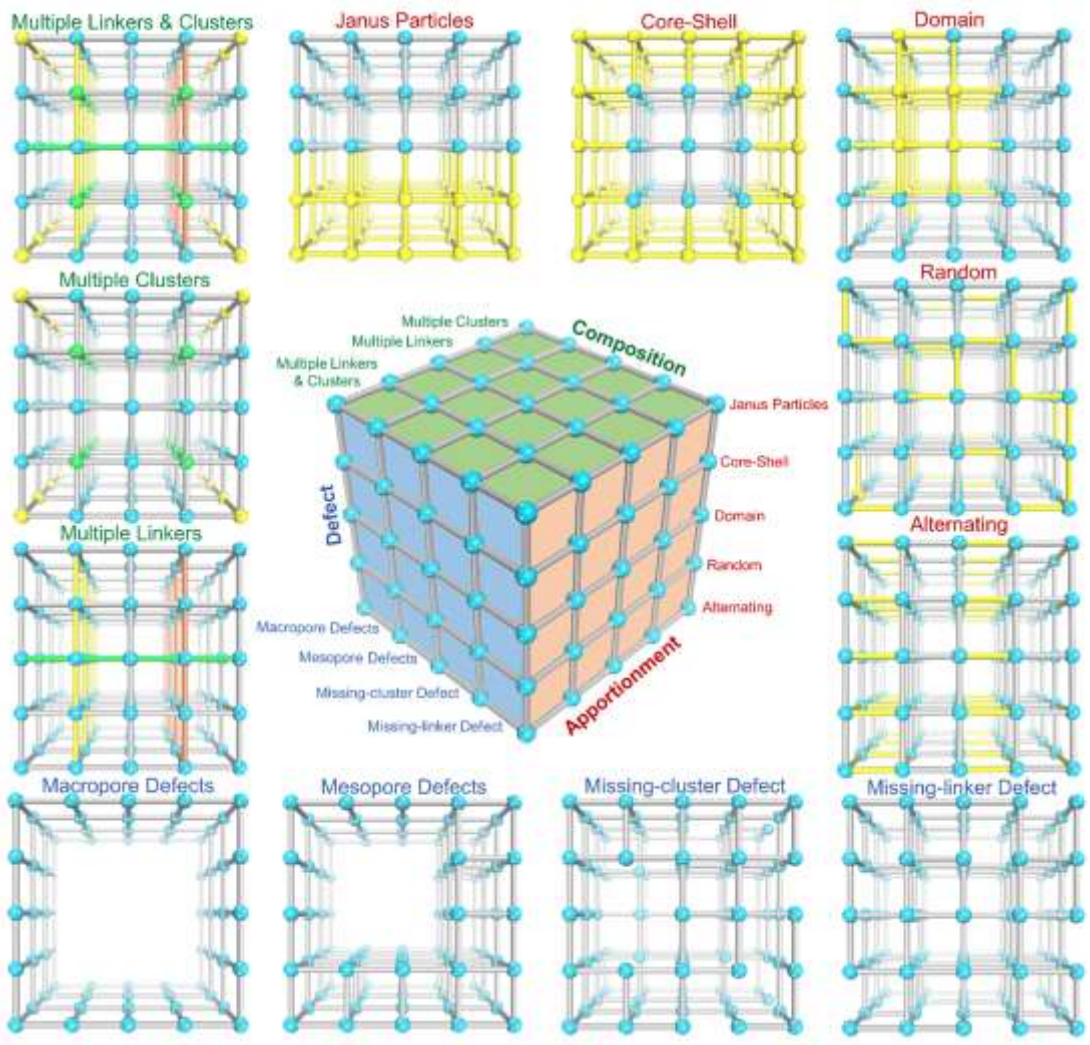

Figure 1. Programmable pore environment in multi-component hierarchical metal-organic frameworks (MOFs). Multi-component MOFs with multiple linkers or/and clusters can be prepared with high tunability (green). Various apportionments of these components, including Janus particles, core-shell, domain, random, and alternating distributions can be prepared by simply tuning the synthetic conditions (red). Defect engineering in MOFs, including missing-linker defects, missing-cluster defects, mesoporous, and macroporous defects lead to the formation of hierarchically porous materials under sophisticated multi-level control (blue).

As well-established classes of porous materials, metal-organic frameworks (MOFs), covalent-organic frameworks (COFs), metal-organic cages (MOCs) and porous organic cages (POCs) have attracted great attention in the last two decades.[6-11] Their permanent pores, often in the nanometer scale, provide ideal spaces for molecular recognition, chemical storage, and the directed conversion of substrates. Additionally, their modular nature imparts designable topologies, adjustable porosities, tunable functionalities, and variable surface moieties within a single material, which allows for a variety of potential applications in many areas, including gas storage, separation, and catalysis.[12, 13] The quest for sophisticated functionalities in framework materials and their related composites typically requires hierarchical structures and specific sequences of multiple building units within the crystal.[14, 15] In particular, MOFs have been targeted due to the ease of introducing synergistic effects originating from the alignment and apportionment of specific functional groups in the proper proximity, something that is highly desired for areas such as cooperative catalysis. To expand upon these ideas, new synthetic methodologies geared towards precisely engineering heterarchy and hierarchy are urgently needed.

Heterarchy, also known as heterogeneity, requires the construction of complex structures with multiple organic and/or inorganic components.[16] The heterarchical features of porous framework materials allow them to operate in parallel on the molecular level due to the specific functionalities compartmentalized within their structures (**Figure 1**). Usually, MOFs are prepared through the self-assembly of metal ions and organic ligands under solvothermal conditions in a "one-pot" reaction, and while this facile and effective method has led to the discovery of numerous framework materials, it possesses inherent limitations. The generation of complex frameworks with multiple ligands or metals in a one pot

reaction remains difficult as these structures tend to be less symmetric and therefore stable, with many multicomponent "one-pot" syntheses resulting in a mixture of MOF products. At that same time, multi-component framework materials show promise for advanced applications, particularly in catalysis, where having multiple functional groups in close proximity can result in alteration of products or product ratios. In addition, the "one-pot" method is less effective for the preparation of stable frameworks with inert metal–ligand (M–L) bonds.[6] This gap between framework design and synthesis has become a critical limitation: with the "one-pot" solvothermal reaction process essentially being a black box, necessitating new means of rationally designing and building new heterarchical frameworks.

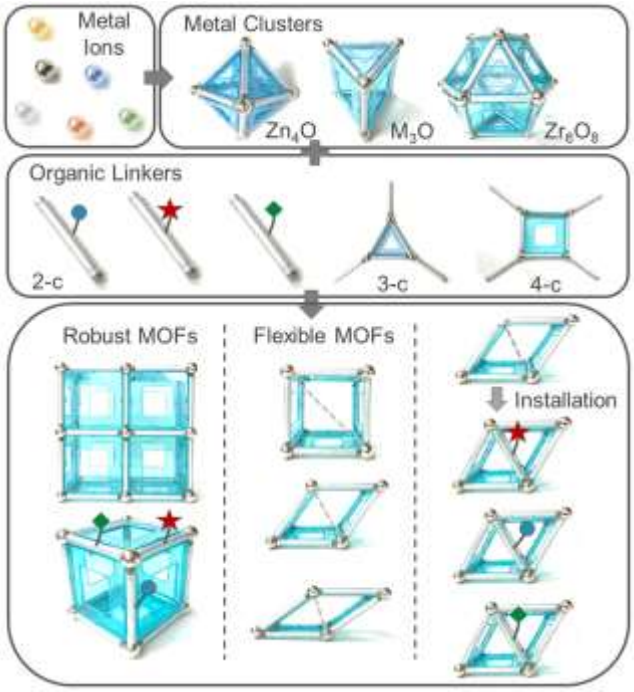

Figure 2. Construction of robust, flexible, or multicomponent MOFs from a library of metal ions/ clusters and organic linkers with various functional groups and connectivities.

Hierarchy refers to the incorporation of multi-level or multi-domain organizations within a system. Hierarchy is well-known within biological systems and is of particular interest for artificial materials.[17] Tuning the hierarchical structure of a material for targeted binding behaviors involves not only optimizing the environment of the binding center, but also improving the selectivity of the porous framework as a whole.[4] This is chiefly done via tuning the order, sequence, and interactivity within the hierarchical network. For example, catalytic activity is primarily focused on the geometry and electronics of the active metal centers, typically using the design philosophies found within homogeneous catalyst design. However, while incorporation of catalytically active moieties within MOFs can allow for improved geometric control, it does also introduce problems associated with the slow diffusion of large reactants into the micropores of the structure. Furthermore, when a microporous framework is used to immobilize bulky catalysts, the active-site accessibility and catalytic activity will plummet due to pore blockage. As such, the incorporation of hierarchical, or multi-scale size, porosity is expected to allow for the well-organized transport of substrates within the pore structures.[18]

With increased attention on expanding the diversity and properties of porous materials, there has been an extensive increase in the study of pore engineering strategies, controlling the compositions, defects, and apportionment within the porous structures (**Figure 1**).[18] The simplest and most efficient method to control these pore structures is through enriching the diversity of metal and linker compositions available for the structures (**Figure 2**). Linkers with various functional groups, with their tunable steric and electronic effects, can be incorporated into the pore walls. Meanwhile metal ions with varying redox activity and Lewis acidity are also able to be integrated at the metal nodes adjacent to the functionalized linkers, allowing for the simple incorporation of tandem methodologies. As such, controlling the arrangement of these structures becomes an important concern for improving their overall performance. Theoretically, when multiple linkers or clusters are incorporated into one framework backbone, they are expected to exhibit one of five common classes of distribution: alternating, random, domain, core-shell, or Janus-particle types. Among these five classes, core-shell and Janus-particle types are usually considered as hierarchical structures due to their macroscopic multi-level arrangement (**Figure 1**). Additionally, defects are another important component for framework materials. Missing-linker or missing-cluster defects can also lead to the colossal changes in adsorption or catalytic properties. When there are mesoporous or macroporous defects created inside a traditional microporous material, the resulting material is dubbed a hierarchically porous materials, as the defects result in secondary domains of pores that can affect diffusion and transportation. The apportionment of these multi-level defects

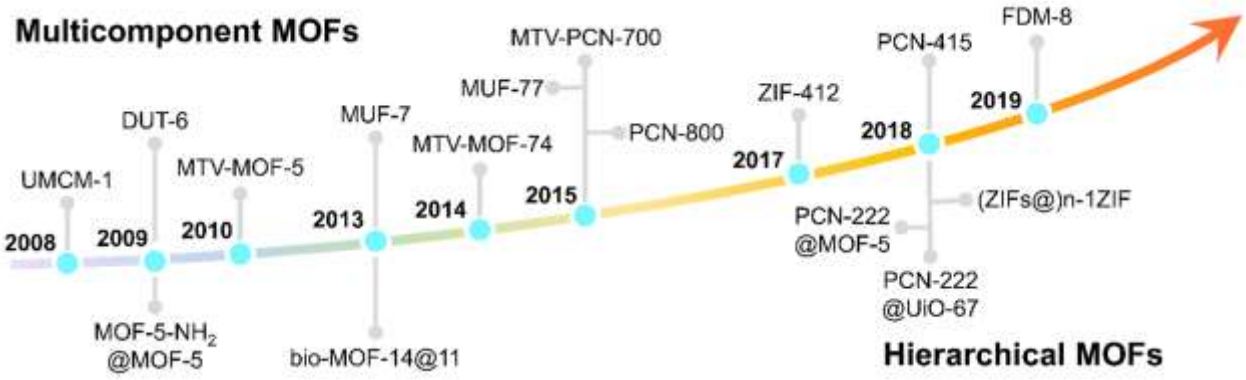

Figure 3. Benchmark examples in the field of multi-component hierarchical MOFs. Several significant discoveries in multicomponent MOFs (above the line) and hierarchical structures (below the line) that utilize multiple variates and varying levels of diversity and order.

dispersed inside the frameworks is also vital for enhancing our understanding on the fundamentals of molecular diffusion within these framework materials.

2 The Chemistry of Multi-component and Hierarchical MOFs

2.1 Synthesis of MOFs with multiple linkers

2.1.1 One-pot synthesis of multi-component MOFs with mixed linkers

The concept of multivariate synthesis involves the introduction of multiple variates (linkers or clusters) into the framework without altering the topology. One of the earliest examples of MTV-MOFs is MTV-MOF-5 developed by Yaghi and coworkers, which incorporated up to eight functionalities into one crystalline network (**Figure 3-4**).[19] The eight functionalities are randomly distributed throughout a framework with an ordered backbone consisting of zinc oxide and phenylene units. Complex MTV-MOF single crystals could be constructed from 1,4-benzenedicarboxylate (BDC) and its functionalized derivatives -NH_2, -Br, -$(Cl)_2$, -NO_2, -$(CH_3)_2$, -C_4H_4, -$(OC_3H_5)_2$, and -$(OC_7H_7)_2$ through a simple one-pot synthesis. The precise linker ratios were accessed by the ^{1}H NMR spectra of an acid digested solution of the MTV-MOF solid. This multivariate strategy could be universalized and extended to a larger MTV-MOF family. For example, highly porous MTV-MOF-177 (Zn), composed of a triangular 1,3,5-benzenetribenzoate (BTB) linker, and its derivates could be synthesized under one-pot conditions, although the formation of new phases and topologies were observed when certain positions on the BTB ligand were functionalized with particular groups.[20]

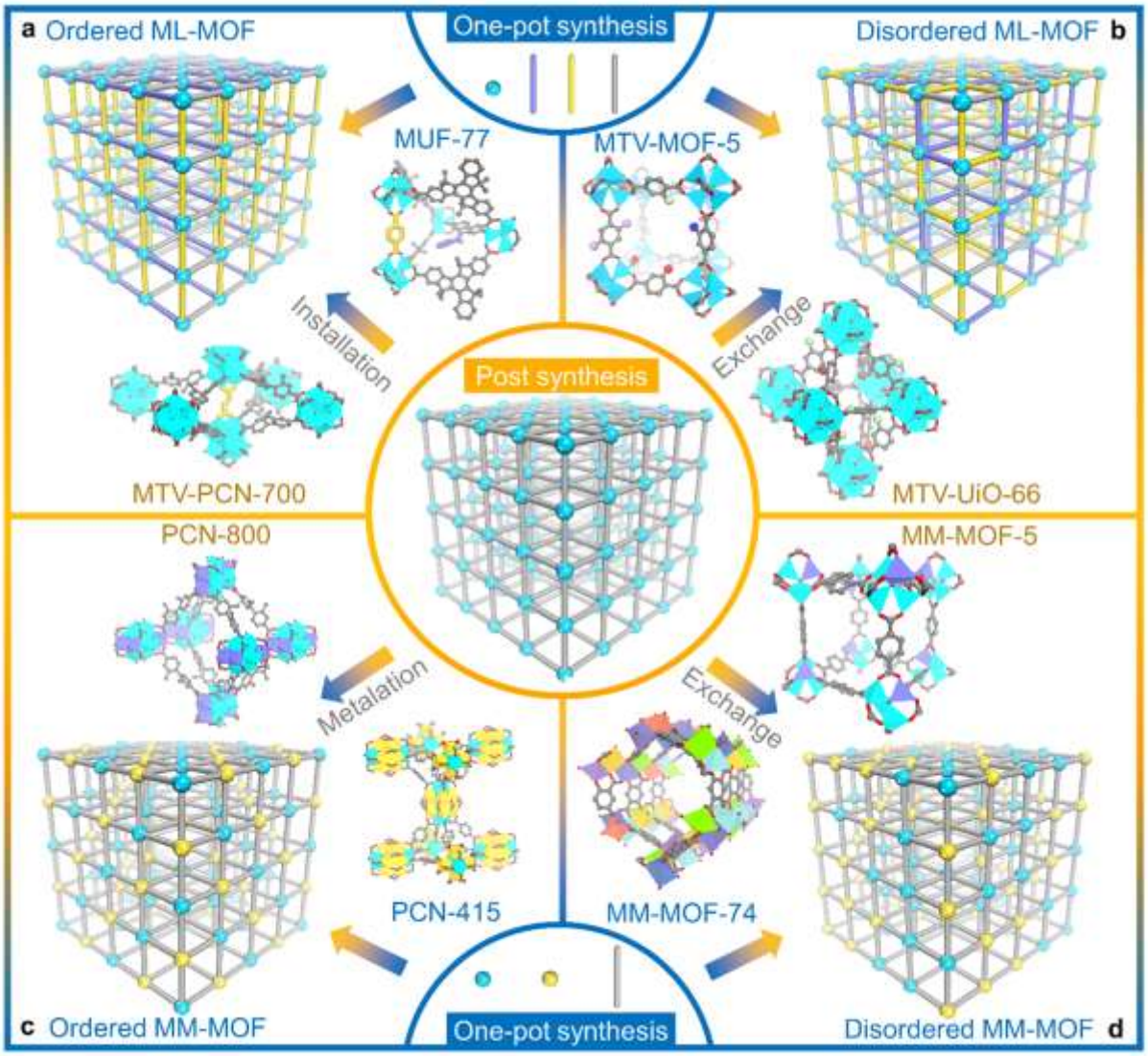

Figure 4. One-pot and post-synthesis of multi-component MOFs. a. Prototypical examples of ordered mixed-linker MOFs: MUF-77 prepared from a one-pot synthesis and a post-synthetically prepared MTV-PCN-700; b. Prototypical examples of disordered mixed-linker MOFs: MTV-MOF-5 prepared from a one-pot synthesis and post-synthetically prepared MTV-UiO-66; c. Prototypical examples of ordered mixed-metal MOFs: PCN-415 prepared from a one-pot synthesis and a post-synthetically prepared PCN-800; d. Prototypical examples of disordered mixed-metal MOFs: MM-MOF-74 prepared from a one-pot synthesis and a post-synthetically prepared MM-MOF-5.

Multiple functionalized linkers can also be installed into the Zr-based UiO-66 [$Zr_6O_4(OH)_4(BDC)_6$] through a one-pot synthesis. Yaghi and coworkers reported a composite Pt⊂UiO-66-S,N, where 2.5 nm Pt NPs were embedded into UiO-66 built from organic linkers with both strong (sulfonic acid, $-SO_3H$) and weakly (ammonium, $-NH_3^+$) acidic functionalities.[21] The resulting structures, showcasing the power of the multivariate strategy, had altered selectivity for the conversion of methycyclopentane to different olefin and hydrocarbon species, with Pt⊂UiO-66-S having a higher preference for cyclohexane production versus benzene production with Pt⊂UiO-66-S,N. Looking at linker based MTV-MOFs as a method of altering the porosity of a structure, MTV-MIL-101 (MIL = Material Institut Lavoisier) is a series of robust and mesoporous MOFs constructed by incorporating multiple functionalities, such as -H, $-NH_2$ and $-C_4H_4$, onto the ligand scaffold.[22] The pore environment could be well tuned by introducing varying ratios of those functionalized linkers, which they used to show the precisely controlled release of the guest molecules rhodamine, ibuprofen, and doxorubicin. The change in release rate was based solely on the functional group incorporated in the MOF and showed the applicability of the MTV-MOF strategy towards drug delivery applications. Cui and coworkers established a series of chiral MTV-MOFs based on mixed metallosalen or M(salen) ligands (M = Mn, Co, Fe, VO, Ru, Cu and Cr).[23, 24] The resulting isostructrual and interpenetrating MTV-MOFs contained cooperative metallosalen active sites which were used for sequential asymmetric alkene epoxidation and epoxide ring-opening

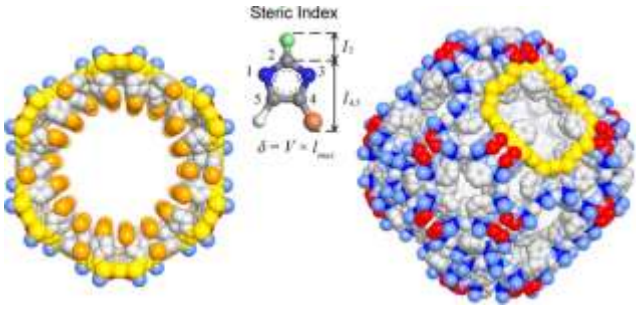

Figure 5. Steric index (δ), related to the size and shape of the imidazolate linkers, was employed in the synthesis of mixed-linker ZIFs with extra-large pore windows. Reprinted with permission from ref. 33. Copyright©2017, American Chemical Society.

reaction, showing the benefits of MTV-MOFs as ideal platforms for these sequential reactions.

The abovementioned MTV-MOFs are constructed from linkers that possess the same length and connectivity yet bear varying functional groups. However, linkers with various lengths and connectivities can also be incorporated into MTV-MOF structures. Our group reported the preparation of MTV-UiO-66-TCPP, which is constructed from 4-connected TCPP ligands and 2-connected BDC ligands.[25] The successful synthesis is contributed to the high symmetry and connectivity

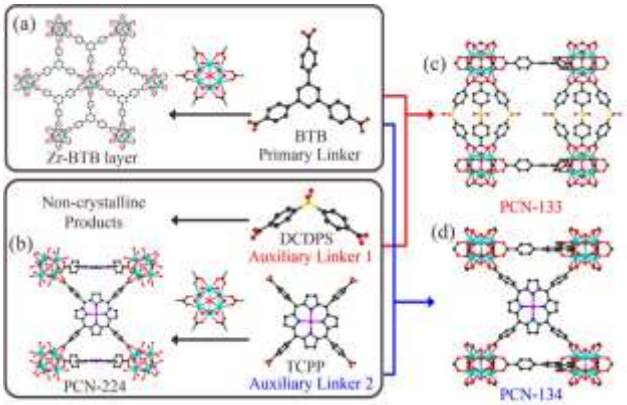

Figure 6. Construction of mixed-linker PCN-133 and PCN-134 through a pillar-layered strategy. Reprinted with permission from ref. 34. Copyright©2016, American Chemical Society.

of the Zr_6 cluster, which enables UiO-66 to preserve its three-dimensional framework even though some BDC ligands are partially replaced by TCPP ligands. Meanwhile, the relatively low concentration of TCPP in the synthesis prevents the initial nucleation and growth of impure phases. This *in situ* one-pot synthetic approach provides a facile route to introduce mixed ligands of different geometries and connectivities into robust and chemically stable MOFs.

The assembly of MTV-MOFs with complex and well-ordered pore architectures can also be achieved through using a series of topologically distinct linkers bearing various functional groups. The Matzger group reported a crystalline mesoporous MOF, UMCM-1 $Zn_4O(BDC)(BTB)_{4/3}$ (UMCM = University of Michigan Crystalline Material), which is constructed from a tricarboxylate and a dicarboxylate linker and a Zn_4O cluster.[26] Further complexity was achieved by the Telfer group, where a quaternary MOF, MUF-7 (MUF = Massey University Framework), was constructed from Zn_4O clusters, 3-connected BTB linkers, as well as 2-connected BDC and BPDC linkers (**Figure 4a**).[27] The resulting framework $[Zn_4O(btb)_{4/3}(bdc)_{1/2}(bpdc)_{1/2}]$ contains a precise combination of linker backbones, that allows for greater control of functional group incorporation in the MOF, as each linker is tunable and exists in a precise relationship with other linkers within the MOF. Systems such as these allow for a good degree of tunability within their frameworks, particularly through the elongation or shortening of the linkers. For example, the combination of BTB and NDC linkers with a Zn_4O cluster gives rise to a highly ordered framework MOF-205;[28] while the combination of TATAB, BDC/NDC/BPDC and Zn_4O leads to the formation of the ST-1, 2 and 4 series (ST = ShanghaiTech University; TATAB = 4,4′,4″-*s*-triazine-1,3,5-triyltri-*p*-aminobenzoate; NDC = naphthalene-dicarboxylate).[29] A new quaternary MOF, ST-3, can also be constructed from Zn_4O clusters, BDC, BPDC, and tritopic TATAB linkers. It should be noted that during the one-pot synthesis of mixed-linker MOFs, compatible length and angles are usually required for the generation of an extended framework. For example, when the

incompatible linkers BPDC and BTB are connected to Zn_4O clusters, no crystalline product will be obtained due to the poor size match between the linkers and clusters.

Feng, Bu, and coworkers reported the pore space partition in a series of M_3O based MOFs through linker installation.[30] For example, CPM-12 (In) based on $[In_2(OH)]_n$ chains was prepared with two tritopic linkers of different sizes: BTC and BTB (CPM = Crystalline Porous Material; BTC = benzene-1,3,5-tricarboxylate).[31] CPM-33 (Ni) is a mixed-linker MOF based on 9-connected Ni_3O clusters with three axial positions coordinated by pyridyl units.[32] More complicated assembly phenomena were discovered during the design and synthesis of mixed-linker ZIFs (ZIF = zeolitic imidazolate framework).[33] It was found that the steric index, a parameter related to the size and shape of various linkers, was vital for the design of MTV-ZIFs with extra-large pore apertures and cages. For example, the combination of three imidazolates (IM, mIM and nbIM), each with different sizes and shapes, introduced in various ratios, can lead to the formation of three different mixed-linker ZIFs: ZIF-486, ZIF-376 and ZIF-414 with cage sizes of 22.6, 27.5, and 45.8 Å, respectively (**Figure 5**).

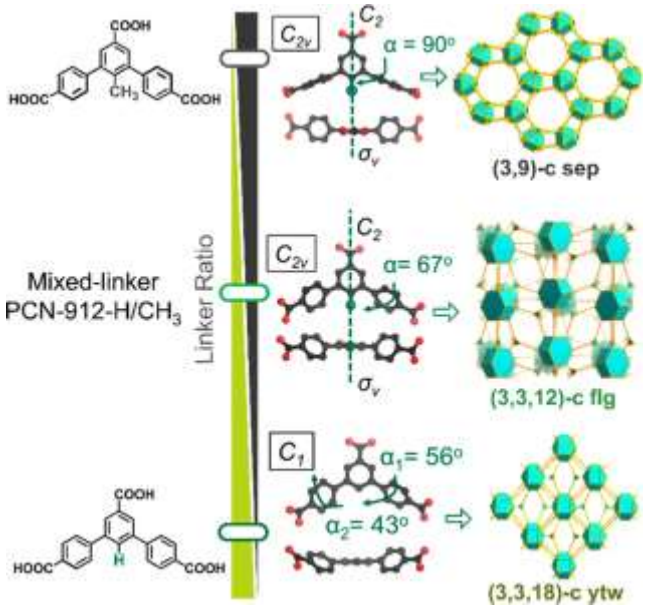

Figure 7. Continuous tuning of linker steric hindrance through the mixed-linker strategy. Reprinted with permission from ref. 37. Copyright©2019, American Chemical Society.

However, the one-pot synthesis of high-valent metal containing MTV-MOFs remains challenging, as the robust metal-ligand bonds in these systems typically limit the coordinative reversibility needed to form ordered MOFs. Therefore, rational design is usually required to obtain an ordered MTV-MOF constructed from high-valent metals. Our group has reported two mixed-linker Zr-MOFs, PCN-133 and PCN-134, possessing a layer-pillar structure (**Figure 6**).[34] A (3,6)-connected **kdg** layer was first constructed from Zr_6 clusters and BTB linkers, which could be further extended into a three dimensional network by auxiliary DCDPS or TCPP linkers (DCDPS = 4,4'-dicarboxydiphenyl sulfone). Rare-earth (RE) metal-based clusters are also a suitable building unit for the construction of MTV-MOFs with multiple functionalities. A

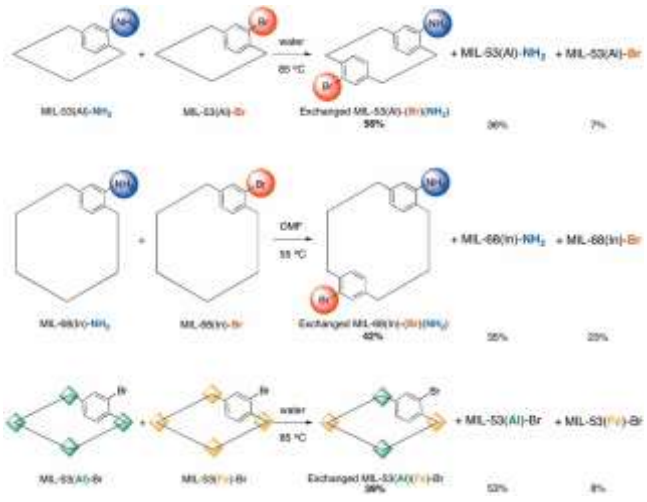

Figure 8. Postsynthetic linker exchange and metal exchange in MIL-53 and -68. Reprinted with permission from ref. 43. Copyright©2012, American Chemical Society.

series of MTV-RE-MOFs, PCN-900(RE), can be obtained using a combination of linear linkers such as BPDC, tetratopic porphyrinic linkers such as TCPP, and $RE_6(OH)_8(COO)_{12}$ clusters.[35] The one-pot formation of PCN-900 takes advantage of a possible PCN-224 isoreticular intermedia, allowing for the *in situ* installation of linear linkers into the open pockets. The Edddaoudi group reported a merged-net approach to prepare RE-MOFs with multiple distinct linkers.[36] The combination of twelve-connected RE_6 clusters, 3-c tritopic linkers, and 6-c hexatopic linkers allowed for the formation of a series of MTV-MOF showing **sph** topology, which can be viewed as the merger of two 3-periodic nets, **spn** and **hxg**. By judiciously combining 3-c tritopic linkers with both small and bulky substituents through mixed-linker strategies, an RE_9-based PCN-912 with a (3,3,12)-c **flg** topology could be accessed as a result of continuous steric hindrance control (**Figure 7**).[37] These studies provide design guidelines for the development of MTV-MOFs for a broad range of metal-ligand interactions as well as a wide distribution of linker connectivities.

2.1.2 Postsynthetic methods to prepare multi-component MOFs with mixed linkers

Although one-pot synthesis is a direct and facile method to construct MTV-MOFs, it is unfavorable when linkers with chemically labile groups need to be incorporated into the ordered stable framework. The synthesis of highly stable MOFs, such as those based on Al, Fe, Cr, and Zr, typically require harsh synthetic conditions which might decompose the chemically labile linkers during MOF synthesis.[6] An alternative method is the utilization of post-synthetic techniques, for example post-synthetic or solvent-assisted linker exchange

under mild conditions, which can potentially protect chemically labile linkers from decomposition (**Figure 4b**).[38-42] Cohen and coworkers demonstrated that linker exchange can occur in robust, topologically distinct MOFs, including MIL-53(Al), MIL-68(In), UiO-66(Zr), and ZIFs under relatively mild conditions (**Figure 8**).[43] Rosi and coworkers reported a post-synthetic ligand exchange process that can be conducted sequentially, resulting in a series of mono-, di-, and trifunctionalized mesoporous MOFs, the bMOF-100 series.[44, 45] The installation and modification of three orthogonal functional groups in the bMOF-100 scaffold highlights the degree of functional complexity within the system. Cui and coworkers reported a series of chiral Zr-based UiO-68-M(salen) through post-synthetic linker exchange.[24] Through a single or multi-step linker exchange process, UiO-68-M(salen), incorporating various metal centers, can be successfully prepared, while the traditional one-pot method failed to achieve the desired product. Depending on the lability of the metal-ligand bonds in the MOF, linker exchange can even be conducted when the exchanged linkers show slightly longer lengths. Rosi and coworkers illustrated that porosity gradients could be established within bMOFs using this partial post-synthetic ligand exchange.[45] The isoreticular pore expansion of mesoporous bMOF-100 could be performed in a stepwise manner, with the system exhibiting a diffusion-limiting behavior. As a result, descending porosity gradients, going from the shell to the core, could be achieved in a partially exchanged bMOF-100.

However, the control of functional group distributions through linker exchange in MOFs is highly dependent on the diffusion and exchange rates of the linker through the MOF channels. For example, Nair and coworkers studied the structural differences in mixed-linker ZIF-8-90 synthesis by linker exchange and one-pot synthesis, with both ZIF-8 and ZIF-90 exhibiting SOD topology and constructed from similarly sized linkers (2-methylimidazole (2-MeIm) and imidazole-2-carboxaldehyde (OHC-Im), respectively (**Figure 9**).[46] The linker exchange process from ZIF-8 → ZIF-90 undergoes diffusion-limited behavior, which leads to the formation of core (ZIF-8)–shell (ZIF-90) morphologies. In contrast, the one-pot mixed-linker synthesis gives rise to well-mixed ZIF-8-90 structures. Similar diffusion-controlled linker exchange processes have also been studied by Matzger and coworkers in a MOF-5 prototype.[47] They found that during the exchange from MOF-5-BDC → MOF-5-BDC-d_4, the exchanged ligand, BDC-d_4, is concentrated at the edges of the crystal as determined by Raman maps, indicating the formation of a core–shell structure. Further diffusion studies demonstrated that the limited diffusion, possibly originating from the hydrogen bonding of the linker to the metal cluster, might be ultimately responsible for the core–shell structure formation. However, in other cases, both linkers were found to be well mixed throughout MTV-MOFs after exchange. Ott and co-workers showed a well-mixed distribution, as determined by Rutherford backscattering spectrometry, when bulkier iodine containing linkers were used for the exchange.[48] Overall, the mechanisms of post-synthetic linker exchange and the related linker diffusion issues are still far from fully understood. Advanced characterization methods are needed to decrypt linker exchange mechanisms, which might inspire the community to develop new routes to better control the apportionment of multiple functionalities inside these frameworks.

Figure 9. Linker exchange leads to the formation of hierarchical core-shell ZIF-8@ZIF-90 structures. Reprinted with permission from ref. 46. Copyright©2017, American Chemical Society.

Post-synthetic linker installation also presents a powerful method to precisely control the placement of functional groups into predetermined positions. Our group previously demonstrated the kinetically controlled installation of linear linkers into a coordinatively-unsaturated Zr-MOF, PCN-700. PCN-700, containing eight-connected $Zr_6O_4(OH)_8(H_2O)_4$ clusters, contains "pockets" for the accommodation of linear linkers with suitable lengths (**Figure 4a**).[49, 50] Based on geometrical analysis, linkers with different lengths were selected and then installed into a parent PCN-700, leading to the formation of MTV-MOFs with up to three different functional groups in predefined positions. A similar phenomenon has also been reported by Su and coworkers, where the same scaffold was utilized to place various functional group containing linkers.[51]

Pore-environment complexity can be further enhanced when linker symmetry is reduced. Zhang and co-workers reported the insertion of three linkers with various lengths into a Zr-MOF, namely NPF-300 (NPF = Nebraska Porous Framework), giving rise to a quinary MOF with precisely placed functionalities .[52] In this case, the flexibility of the tetratopic primary linker ensures that the linker is capable of distortion after insertion. A trapezoidal linker of C_s symmetry was used by our group to generate a MOF, PCN-609, with low symmetry.[53] As a result, PCN-609, with three crystallographically distinct pockets, can be used to accommodate three linear linkers of various lengths, creating unprecedented multivariate pore environments.

This post-synthetic crystal engineering allows for the construction of complicate structures with atomic level precision. Attempts to reach the same level of sophistication as organic synthesis have been made, for example, in the case of PCN-201 and 202, which were developed based on organic retrosynthetic techniques.[54] Based on retrosynthetic design

principles, multi-step reactions should begin with the formation of the most robust coordination bonds, as they require the harshest reaction conditions. The other components should then be subsequently installed onto the framework through the formation of more labile coordination bonds under mild condition. Eventually, four quaternary MOFs composed of up to two different linkers and three different metals were synthesized, with all components arranged in a predetermined array within the lattice.

2.2 Synthesis of MOFs with multiple metals

2.2.1 One-pot synthesis of multi-component MOFs with mixed metals

MTV-MOFs with mixed metals are relative rare compared to mixed-linker MTV-MOFs, as it is much easier to generate multiple MOFs or amorphous phases during the nucleation and growth process. The various metal coordination modes also bring structural design challenges, with the mixed metal

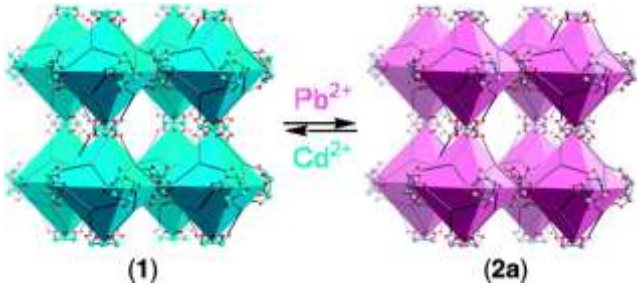

Figure 10. Metathesis in Pb-MOF and Cd-MOF single-crystals: complete and reversible metal exchange can be achieved through post-synthetic methods. Reprinted with permission from ref. 65. Copyright©2009, American Chemical Society.

systems needing to have similar coordination ability and affinity. Yaghi and coworkers reported the one-pot synthesis of a mixed-metal MOF-74 containing up to ten different kinds of metals (Mg, Ca, Sr, Ba, Mn, Fe, Co, Ni, Zn, and Cd) within a single crystal (**Figure 4d**).[55] These metal ions are heterogeneously distributed within each of the crystalline particles as indicated by Energy-dispersive X-ray spectroscopy (EDXS). Similar well-mixed distribution phenomenon have also been observed in cases such as PCN-600 or $(M_3O)_2(TCPP)_3$ (M = Mg, Mn, Co, Ni and Fe).[56] It was found that Fe and Ni ions are well-mixed in the M_3O clusters of PCN-600 as the similarities between Ni^{2+} and Fe^{3+} permits their concurrent presentation in the same cluster. However, the metal spatial arrangement in PCN-600(Fe, Mn) was observed to exist in the form of separate domains, rather than well-mixed, due to the significant differences in coordination behavior between Mn^{2+} and Fe^{3+}. The combination of various metals in M_3O clusters has also been reported by Feng, Bu, and coworkers. Heterometallic CPM-200s (also known as PCN-250) built from metal ion combinations such as Mg/Ga, Mg/Fe, Mg/V and Mg/Sc have shown unexpected synergistic effects for gas sorption.[57]

Although the preparation of MTV-MOFs with more than two metal clusters in one ordered structure is challenging, some recent progress has shown that rational design and targeted synthesis in this area is achievable. In the work of Zaworotko and coworkers Cr_3O clusters are synthesized with pyridyl groups as terminal ligands, and subsequently linked to various metal clusters and organic linkers to construct heterometallic MOFs.[58] Bifunctional linkers are typically required to obtain ordered mixed-metal MOFs in one-pot synthesis, as the different functional groups in the linkers can distinguish between the metal ions in solution through Pearson's hard/soft acid/base (HSAB) principle. Li and coworkers showed that the incorporation of multiple distinct inorganic clusters (Cu/Zn) could be achieved in one structure, FDM-4-7 (FDM = Fudan material), through the use of copper pyrazolates as metalloligands which are connected to Zn_4O carboxylate clusters to form an extended framework.[59] Guided by the HSAB principle, Yuan and coworkers demonstrate the first example of a heterometallic cluster-based Zr-MOF, which is assembled from tetrahedral $[Cu_4I_4(INA)_4]^{4-}$ (INA = isonicotinate) metalloligands and 8-connecting $[Zr_6(\mu_3\text{-}OH)_8(OH)_8]^{8+}$ clusters.[60] The Rosi group reported a series of MTV-MOFs built from hard-acid metal clusters (Zr^{4+}, Hf^{4+}, Dy^{3+}), a second softer metal cluster (Co^{2+}, Cu^{n+}, Ni^{2+}, Fe^{3+}, Cd^{2+}) and a bifunctional isonicotinate linker.[61] For example, MOF-1210(Zr/Cu), constructed from Zr_6 clusters and Cu-(2-methyl-INA)$_2$ complex linkers, can be synthesized under mild one-pot synthetic conditions. Using similar principles, the bimetallic MOF-818(Zr/Cu) can also be built from hard-acid Zr clusters, soft-acid Cu clusters, and a small ditopic organic linker, 1H-pyrazole-4-carboxylic acid (H_2PyC).[62] Remarkably, in the bimetallic MOF-919(Fe/Cu), the largest cage, with a diameter of 6.0 nm, exhibits a cage size to linker size ratio of 15, which is a promising size ratio for biomolecular capture applications. Recently, FDM-8, a MOF with two distinct metal clusters and three distinct carboxylate and pyrazolate linkers was constructed, achieving a high level of control over MOF complexity and functionality.[63]

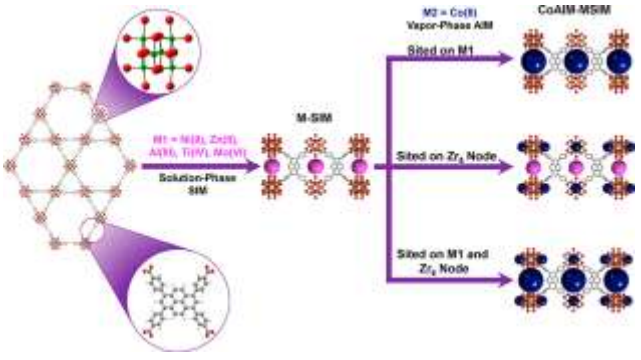

Figure 11. Control over the composition and activity of NU-1000-supported bimetallic catalysts (NU = Northwestern University). NU-1000 with anchored Co ions exhibits outstanding activity for the oxidative dehydrogenation of propane. Reprinted with permission from ref. 70. Copyright©2017, American Chemical Society.

Another possibility for the construction of ordered MTV-MOFs with multiple metal species is to introduce a preformed and stable bimetallic cluster during the synthesis. The stable coordination bonds in the clusters ensures that the cluster remains intact, while also preventing the formation of other impurities. Our group reported a bimetallic, 12-connected decanuclear cluster $[Ti_8Zr_2O_{12}(COO)_{16}]$, and its extended framework structure upon connecting to ditopic linkers such as BDC, leading to a **fcu** net (**Figure 4c**).[64]

2.2.2 Postsynthetic methods to prepare multi-component MOFs with mixed metals

Postsynthetic metal exchange can be easily performed in MOFs to achieve metathesis in a single crystal. Kim and coworkers reported the complete and reversible metal exchange between a Cd-MOF and an isoreticular Pb-MOF (**Figure 10**).[65] The Cohen group further report the metal ion transfer in the robust MOFs, for example, the metal ion exchange between MIL-53(Al) and MIL-53(Fe), and were also able to incorporate Ti into UiO-66(Zr) through exchange with a variety of molecular Ti precursors.[43] However, it should be noted that it was later realized that Ti deposited as TiO_2 on the surface of UiO-66(Zr), rather than yielding the exchanged UiO-66(Zr, Ti), as indicated by inductively coupled plasma mass spectrometry and transmission electron microscopy.[66]

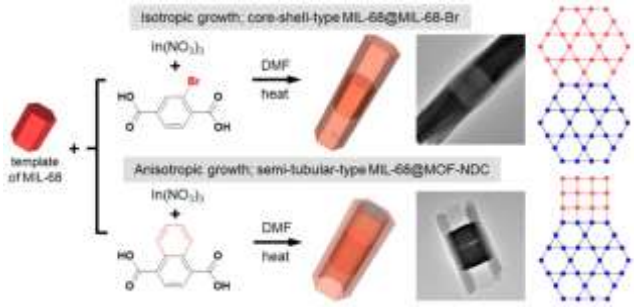

Figure 12. Growth of MIL-68-Br and MOF-NDC on the crystal seed MIL-68. Core–shell MIL-68@MIL-68-Br and semitubular-type MIL-68@MOF-NDC were obtained via isotropic and anisotropic growth. Reprinted with permission from ref. 77. Copyright©2016, American Chemical Society.

Due to the complexity of heterobimetallic MOF synthesis, the post-synthetic modification of parent MOFs might provide an alternative approach to precisely control the generation of "layer-on" metal clusters. For example, when reacting with M^{2+}, the 8-connected $[Zr_6O_4(OH)_8(H_2O)_4]$ cluster in the Zr-based PCN-700 tends to undergo cooperative metalation and ligand migration, generating a bimetallic $[Zr_6M_4O_8(OH)_8(H_2O)_8]$ cluster in the MOF (**Figure 4c**).[67] The Hupp and Farha group also demonstrated that the -OH sites on the Zr_6 clusters of UiO-66 could be metalated with various metal ions such as redox-active V^{5+} ions for catalysis.[68] Additionally, gas-phase atomic layer deposition has shown versatility for installing

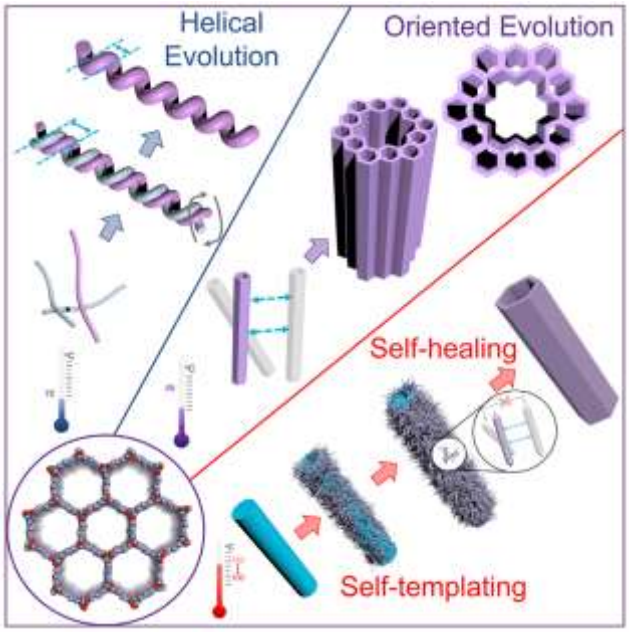

Figure 13. Temperature-controlled evolution of nanoporous MOF crystallites into hierarchically porous superstructures. Reprinted with permission from ref. 81. Copyright© 2019 Elsevier Inc.

isolated metal centers onto Zr_6 nodes, including Ni, Cu, Zn, and Al (**Figure 11**).[69, 70]

More complicated coordination structures can be assembled on robust frameworks through post-synthetic strategies. PCN-160, a Zr-MOF, was synthesized as a scaffold structure and then exchanged with labile linkers. These labile linkers can then be partially removed and replaced by pyridinecarboxylates. As a result, these neighboring pyridyl groups can be placed to form *trans*-binding sites that can accommodate various metal species including Mn^{2+}, Fe^{2+}, Co^{2+}, Ni^{2+}, Cu^{2+}, and Pd^{2+}.[71] Guided by retrosynthetic design, bimetallic MOFs with $MX_2(INA)_4$ moieties (M=Co^{2+} or Fe^{2+}; X=OH^-, Cl^-, Br^-, I^-, NCS^-, or $NCSe^-$) could be obtained by the sequential incorporation of Zr clusters and pyridinecarboxylates, leading to symmetry, unit cell, and topology alterations of the parent structure.[72]

2.3 Construction of multi-component MOFs with hierarchical structures

The construction of MTV-MOFs with hierarchical structures is considered to be a viable method for achieving targeted applications that require sophisticated mesoscopic architecture, such as those involving difficult mass transport, or advanced separations. One of the earliest examples was introduced by Kitagawa and co-workers, where the assembly of a shell Cu-MOF $[Cu_2(NDC)_2(DABCO)]_n$ (DABCO = 1,4-diazabicyclo[2.2.2]octane) on the surface of its Zn counterpart was observed, generating a heterogeneously hybridized MOF.[73, 74] The Matzger group further studied the effects of

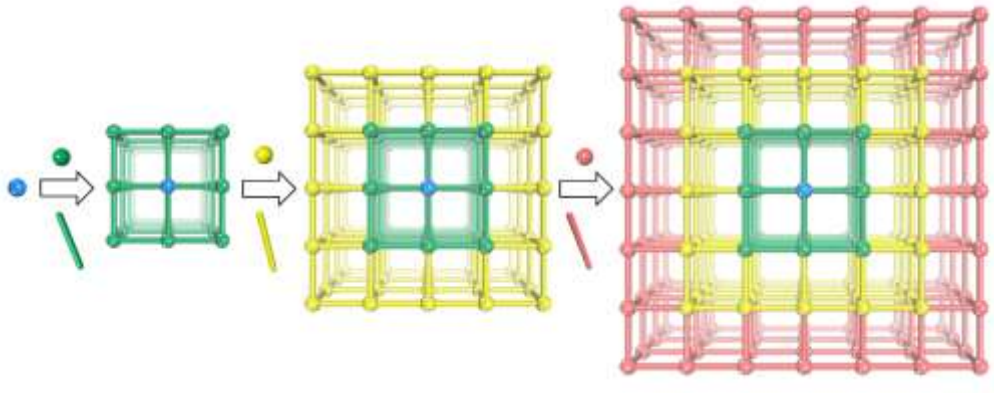

Figure 14. Sequential preparation of multivariate hierarchical MOFs guided by two principles: surface functionalization and retrosynthetic stability considerations. To obtain a desired MTV-MOF, the stepwise synthesis, starting from the more stable bonds and going to the more labile bonds, should be rationally carried out. Controlled post-synthetic installation of metal clusters and linkers on the stable framework leads to the formation of hierarchical MTV-MOFs with multiple compositions, various spatial distributions, and tailored properties.

linker addition sequence on the linker distribution in a resulting core-shell MTV-MOF.[75] Microporous core–shell architectures, for example MOF-5-NH_2@MOF-5, could be obtained when two different linkers were added sequentially into the reaction system. The initially formed MOF-5 crystals can act as seeds, allowing for the epitaxial growth of the shell MOF-5-NH_2. Another representative example, bio-MOF-14@bio-MOF-11, was introduced by the Rosi group, and was synthesized via a similar stepwise synthesis.[76] The resulting hierarchical core-shell MOF exhibited a higher CO_2/N_2 selectivity than bio-MOF-11 and a higher CO_2 storage capacity than bio-MOF-14. The detailed growth mechanism of MOF-on-MOF structures has been illustrated by Oh and co-workers in the case of MIL-68(In).[77] As illustrated by TEM studies, a core–shell MIL-68@MIL-68-Br could be obtained via the isotropic growth of MIL-68-Br on the MIL-68 seeds while semitubular particles of MIL-68@MOF-NDC were synthesized through a unique anisotropic growth of MOF-NDC on the MIL-68 seeds (**Figure 12**). These results enhance our understanding of hierarchical MOF nucleation and growth behaviors, suggesting that cell parameters are important factors that influence the isotropic or anisotropic growth pathways. These successful epitaxial growth processes can also be extended to ZIFs, for example ZIF-8(Zn)@ZIF-67(Co).[78, 79] Since the two representative ZIFs share the same organic linker, MeIm, and the same crystallographic features, the core–shell structured ZIF-8@ZIF-67 and ZIF-67@ZIF-8, and other Matryoshka-type $(ZIFs@)_{n-1}ZIFs$ with 4-8 layers could be synthesized via a stepwise liquid-phase epitaxial growth.[80] Our group recently reported an one-pot assembly of MOF crystallites into helical, multichannel or hollow tubular superstructures based on the lattice matched oriented assembly (**Figure 13**).[81] As such, matched lattice parameters have long been viewed as a requirement for hierarchical MOF-on-MOF hybrid growth. Because most MOFs have distinct crystallographic parameters, the preparation of hierarchical MOFs via epitaxial growth has had severely limited applicability.

Recently, some progress has been made to overcome this lattice matching rule. Kitagawa and coworkers reported the introduction of a polymer into the interface of two MOF phases with different crystallographic parameters.[82] Various MOFs with distinct functions could be combined into a MOF matrix through this internal extended growth method. Our group also demonstrated a one-step synthesis of hybrid core–shell MOFs with mismatching lattices under the guidance of nucleation kinetic analysis.[83] A series of hierarchical MOFs with a mesoporous core of PCN-222 and microporous shell of UiO series MOFs were synthesized during a one-pot reaction. This interesting phenomenon inspired us to expand the scope and complexity of the MTV-MOF family. To enhance control during framework assembly, we proposed a stepwise generation of hierarchical MOF-on-MOF formation under two principles: surface functionalization and retrosynthetic stability considerations (**Figure 14**).[84] As mentioned above, the retrosynthetic design principle requires a stepwise procedure, going from stable bond formation before going to more labile bond formation. Metal–carboxylate bond strengths with a given ligand are proportional to the charges of the metal cations while they are inversely proportional to the ionic radius. Therefore, by checking the strength of the bonds that form the framework, we can roughly predict the stability of the MOFs. It is believed that when it comes to metal–carboxylate frameworks, high-valent metal ions possessing higher charge densities can form stronger coordination bonds, leading to a more stable framework. The controlled post-synthetic installation of metal clusters and linkers on the stable framework leads to the formation of hierarchical MTV-MOFs with multiple compositions, various spatial distributions, and tailored properties.

Further control over the composition and hierarchy inside MTV-MOFs can be achieved (**Figure 15**). For example, a major

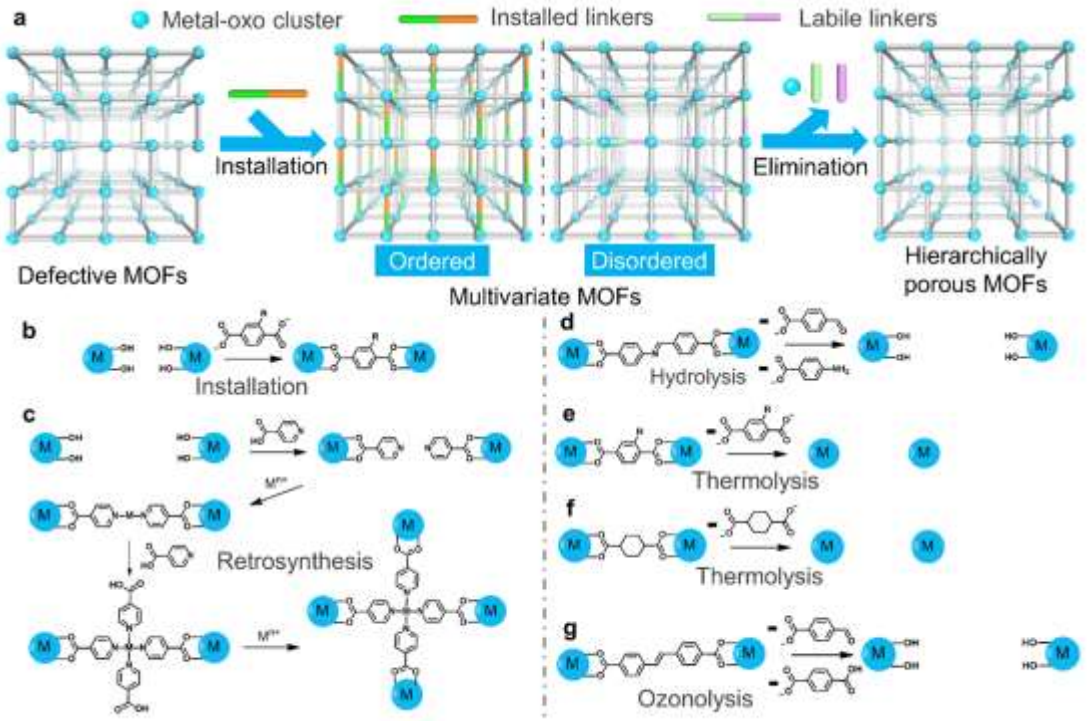

Figure 15. Illustration of the relationship between defective, hierarchically porous MOFs, and multivariate MOFs. a. Generation of ordered multivariate MOFs from defective MOFs via linker installation. Conversely, hierarchically porous MOFs with well-engineered defects can be prepared from multivariate MOFs; b. Linker installation can precisely place linkers into predetermined defective sites; c. Stepwise linker and cluster installation leads to the "total synthesis" of a complex multi-component framework material; d. Linker labilization utilizes the hydrolysis of acid-sensitive linkers to create mesopores and defects insides microporous materials; e-f. Hierarchical pores can be created through linker thermolysis by selectively removing thermolabile linkers with thermolabile functional groups such as -NH_2 (e) or with flexible configurations (f); g. Linker ozonolysis can be utilized to break C=C in robust linkers and generate mesopores insides microporous MOFs.

goal of MOF research is to expand the pore size and volume to allow the immobilization of large molecules such as enzymes and other bulky catalytic species inside the pore space. A powerful strategy, called linker labilization reported by our group, was exploited to create mesopores by generating crystal defects throughout a microporous MTV-MOF (**Figure 15d**).[85] In this case, linker instability, although an undesirable feature of MOFs, can be utilized to construct hierarchical-pore architectures. Zr-MOFs constructed from a robust linker AZDC were first labilized by linker exchange with a pro-labile imine-based linker, CBAB (4-carboxybenzylidene-4-aminobenzate). Under acid treatment, the labile CBAB linker can be dissociated into 4-amino benzoic acid and 4-formylbenzoic acid through hydrolysis, leading to the formation of missing-linker and missing-cluster defects inside the frameworks.[86] The well-controlled labilization can also be carried out in a series of MTV-MOFs containing linkers with various thermal stabilities. The thermal-sensitive linkers in MTV-MOFs can be selectively cleaved via a decarboxylation process, enabling controllable mesopore creation in a series of microporous MOFs (**Figure 15e-f**).[87] The stark contrast between the stability of ordinary linkers such as BDC and thermolabile or flexible linkers such as BDC-NH_2 or trans-1,4-cyclohexane-dicarboxylate (CDC) leads to selective thermolysis.[88] The formation and construction of hierarchical pores are highly related to the linker distributions inside the framework. When rigid linkers are mixed during the one-pot synthesis, for example BDC and BDC-NH_2 in UiO-66, the linkers tend to form some small domains inside the backbone, leading to missing-cluster mesopores after thermolysis (**Figure 15e**). When one rigid linker BDC and one flexible linker CDC are mixed during the one-pot synthesis, the linkers tend to exhibit well-mixed distributions inside the backbone (**Figure 15f**). As a result, no mesopores are observed after thermolysis due to the presence of only missing-linker defects. The construction of mesoporosity in MTV-MOFs can be also accomplished by an ozone-based labilization method (**Figure 15g**).[89] In this case, a robust and ozone-resistant linker and a linker with ozone-cleavable olefin bonds can be incorporated inside the MTV framework, and controllable mesopores can be generated via ozonolysis. These hydrolysis, thermolysis, and ozonolysis methods provide an ideal platform to tailor porosity inside MTV-MOFs for targeted applications.

2.4 Characterization of multi-component MOFs

Understanding the distribution of functionalities throughout the framework is essential for the fundamental study of MOF formation and the "structure-property-application" relationship. Single-crystal X-ray Diffraction (SCXRD) is typically used to obtain detailed information about how different linkers are precisely arranged inside framework. However, an unfortunate drawback to the use of SCXRD is these methods are less effective for disordered systems, as they require highly crystalline and ordered structures in order to gather solvable data. For instance, SCXRD data was used to confirm each of the 11 daughter MOFs in the PCN-700 series after linker installation.49 This was only possible because the technique used to generate the daughter MOFs, post-synthetic linker installation, produced highly ordered structures, if only a limited number of linkers were installed, or if the installation was not well distributed, the SCXRD data would not be solvable.

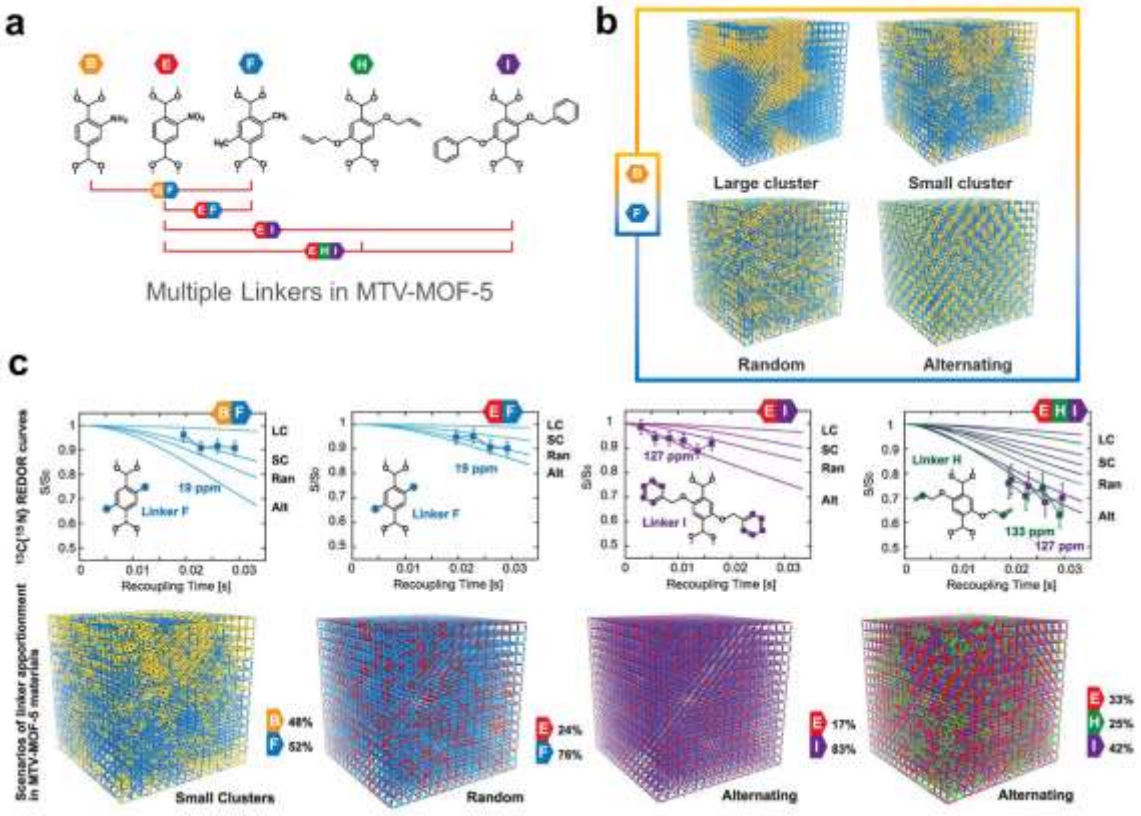

Figure 16. Mapping of functional groups in multivariate MOFs. a. The BDC-X linkers, where X = -H, -NH_2, -NO_2, -$(CH_3)_2$, -$(OC_3H_5)_2$, and -$(OC_7H_7)_2$ in MTV-MOF-5 series; b. Four different distribution models of MTV-MOF-5-BF including large cluster, small cluster, random defects, and alternating defects were studied; c. Mapping functional groups insides MTV-MOFs by the combination of rotational-echo double-resonance (REDOR) NMR results and the molecular dynamics simulations. Reprinted with permission from ref. 92. Copyright©2013, American Association for the Advancement of Science

Nuclear magnetic resonance (NMR), in both solution and solid state, can be used to analyze and quantify the interactions between linker functional groups in MOF samples, and is of particular use in investigating samples of limited crystallinity.[33, 90, 91] Solid state nuclear magnetic resonance (SSNMR) is of particular interest because MOF structures are typically not maintained when dissolved in solution. Additionally, this technique can be combined with computational modeling to characterize the structures within disordered MTV-MOFs such as the MTV-MOF-5 series discussed as part of the one-pot mixed linker strategies (section 2.1, **Figure 16**).[19, 92] This approach opens a new perspective for the characterization of spatially disordered systems inside ordered materials such as MOFs or other mesoporous materials. In MTV-MOF-5 in particular, SSNMR was utilized to determine the heterogeneous mesoscale spatial arrangement of the functional groups in the MTV-MOF-

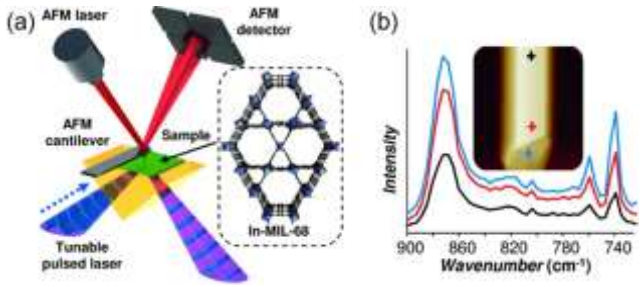

Figure 17. PTIR techniques (a) can be utilized to illuminated the linker distributions in In-MIL-68-NH_2-50%, as indicated by PTIR spectra (b). Reprinted with permission from ref. 93. Copyright ©WILEY-VCH Verlag GmbH & Co. KGaA, Weinheim

5 series containing the BDC-X linkers, where X = -H, -NH_2, -NO_2, -$(CH_3)_2$, -$(OC_3H_5)_2$, and -$(OC_7H_7)_2$ (**Figure 16a**).[19] Different distribution models were then used alongside the data collected by SSNMR to illustrate the linker spatial arrangement, including possibilities of random or alternating cluster forms (**Figure 16b**). However, this information on the average distances and apportionments of linkers and linker domains on the nanoscale still lags behind that gathered by SCXRD, as it does not provide clear and direct spatial information on the linker distribution within a crystal. Additionally, the use of NMR based techniques is typically limited when in the presence of paramagnetic metal clusters, and it can be difficult to study the interaction behavior between functional groups in mesoporous MOFs due to the enlarged distances. In addition to NMR, other techniques, such as visible microscopy and IR spectroscopy can be utilized to reveal structure details such as linker arrangement. While these techniques usually need single crystals larger than 200 µm, and require two linkers in the structure to form distinct phase-separated domains such as the difficult to synthesize core-shell structures. Despite this, these techniques can be instrumental in determining the nature of the interphase boundary. Other characterization techniques, such as photothermal induced resonance (PTIR) have been reported to assess linker gradients within a crystal (**Figure 17**).[93] PTIR is an effective method to elucidate chemical compositions, with

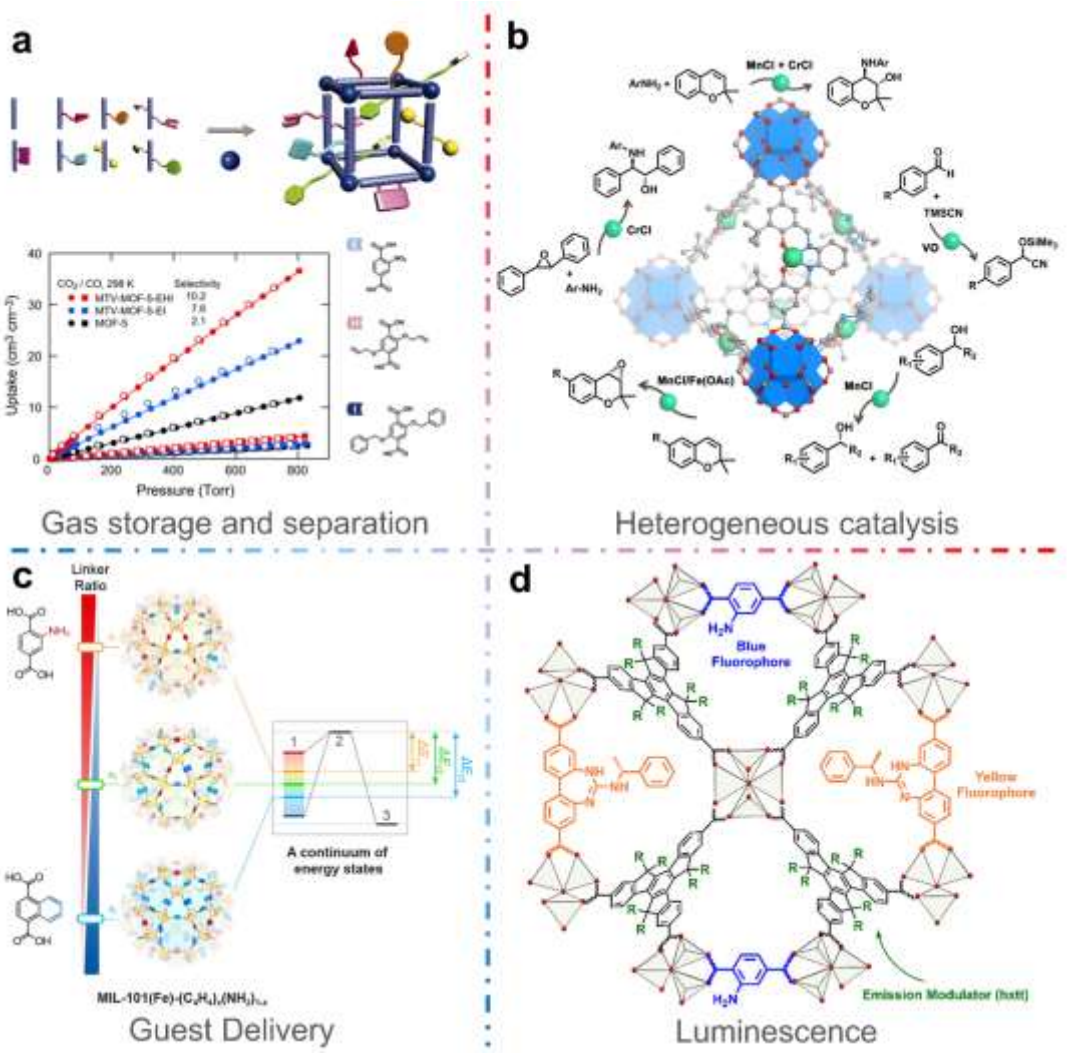

Figure 18. Applications of multi-component MOFs. a. MTV-MOF-5-EHI, where E refers to -NO_2, H refers to -$(OC_3H_5)_2$ and I refers to -$(OC_7H_7)_2$, exhibits up to 400% better selectivity for carbon dioxide over carbon monoxide as compared to MOF-5; b. Sequential asymmetric alkene epoxidation/epoxide ring-opening reactions can be achieved through the well-designed mixed-M(salen) linker based chiral UiO-MOFs; c. Binding energy states of single-component MIL-101 and MTV-MIL-101 for tunable guest delivery kinetics; d. Illustration of the arrangement of multiple linkers in MUF-77 which enable a systematic control over luminescence output. Panel a is reprinted with permission from ref. 19. Copyright©2010, American Association for the Advancement of Science. Panel b is reprinted with permission from ref. 24. Copyright©2018, American Chemical Society. Panel c is reprinted with permission from ref. 22. Copyright ©2017, American Chemical Society. Panel d is reprinted with permission from ref. 96. Copyright©2018, American Chemical Society.

resolutions of approximately 100 nm, but improvements are still needed to achieve mesoscale spatial apportionment. Native-fluorescence confocal microscopy has also been shown to aid in the visualization the linker arrangement ZIF structures, but this technique also requires large crystal and suffers from similar resolution problems as PTIR.[46] The information gained by these new techniques will in turn accelerate the discovery and development of new MTV-MOF structures that contain previously unknown functionalities.

2.5 Applications of multi-component MOFs

2.5.1 Gas storage and separation

Multi-component MOFs containing complex sequences and apportionments within the framework have demonstrated unusual gas storage and separation properties as compared to the parent MOF structures or their linear sum of components. For example, MTV-MOF-5-EHI, where E refers to -NO_2, H refers to -$(OC_3H_5)_2$ and I refers to -$(OC_7H_7)_2$, exhibits up to 400% better selectivity for carbon dioxide over carbon monoxide as compared with MOF-5 (**Figure 18a**).[19] To introduce periodicity into the framework, a version of MUF-77 with ordered functionalities, dubbed "programmed pores" was generated.[94] The CO_2 sorption capacity of the resulting MTV-MOF was enhanced by almost 100% due to the synergistic effects of the new components. PCN-700 (also known as LIFM-28) was installed with several varieties of shorter or longer linkers, allowing it to achieve enhanced performance in multiple areas, including gas separation and storage.[51] For example, these Zr-MTV-MOFs can reach ultrahigh CH_4 storage working capacities at 5–80 bar and 298 K through precise engineering of the positions and concentrations of $-CH_3$ groups. In terms of gas separation behavior, linkers with multiple amine groups, showing strong interactions with CO_2, can be placed inside the framework, leading to the exceptional CO_2/CH_4 and CO_2/N_2 separation selectivities of 9.9 and 34.7, respectively. Hierarchical MOF materials with multi-level control over functionalities can also be utilized for selective CO_2 capture. The Rosi group has reported a hierarchical bio-MOF-11/14 with a porous mixed-linker core and water-stable bio-MOF-14 as a shell.[76] The shell can effectively alter the N_2 and CO_2 adsorption selectivities, allowing for the selective capture CO_2 from a mixture of N_2 and CO_2.

2.5.2 Heterogeneous catalysis

Owing to diverse linker functionalities, complex pore environments, and potential internal cooperative catalytic sites, multicomponent MOFs have demonstrated outstanding performances over other conventional porous materials. For example, MTV-UiO-66-FeTCPP represents a robust and stable platform that can incorporates active porphyrin units into the stable UiO-66 framework, achieving high catalytic activity for the oxidation of 2,2'-azino-bis(3-ethylbenzthiazoline-6-sulfonic acid (ABTS) in the presence of H_2O_2.[25] Further chemical environment control can be achieved in the system of Pt⊂UiO-66-S,N, where the controlled environment results in a unique alteration of the selectivities for the gas-phase conversion of methylcyclopentane (MCP) to cylic and acyclic derivative species, including olefins, cyclohexane, and benzene (**Figure 19**).[21] For instance, Pt⊂nUiO-66-S achieves a doubled catalytic activity compared with the non-functionalized Pt⊂nUiO-66 and the highest selectivity to C_6-cyclic products without observed acyclic isomers products, while the selectivity for C_6-cyclic products was decreased to <50% and the selectivity for the acyclic isomer was increased to 38.6%, in the case of Pt⊂nUiO-66-N. With the mixed-linker Pt⊂nUiO-66-SN, benzene was the dominant product while only minor olefins and acyclic isomers were produced, with no cyclohexane

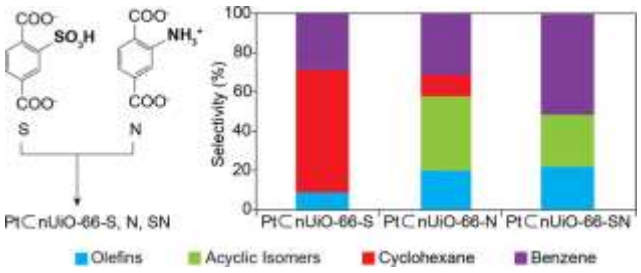

Figure 19. Control over chemical environment in mixed-linker Pt⊂nUiO-66-SN leads to enhanced catalytic selectivity of gas-phase methylcyclopentane (MCP) conversion. Reprinted with permission from ref. 21. Copyright©2015, American Chemical Society.

observed. The results demonstrate the complicate catalytic behaviors within the systematically functionalized MOF pore environments. Cooperative catalytic process have been further achieved in the mixed-M(salen) linker based chiral UiO-MOFs (**Figure 18b**).[24] Sequential asymmetric alkene epoxidation/epoxide ring-opening reactions was achieved through the well-designed and versatile heterogeneous catalysis.

For MTV-MOFs with ordered linker distributions, the precise and systematic modulation of pore volume and environment is achievable by a judicious selection of linkers, resulting in a highly dynamic multifunctional catalytic system capable of complex cooperative behavior. For example, an MTV-PCN-700 installed with catalytic unit BPYDC(Cu) (BPYDC = biphenyl-5,5'-dicarboxylate; TPDC = [1,1':4',1''-terphenyl]-4,4''-dicarboxylate) and size-control unit TPDC-R_2 (R = Me, Ph, or Hex) can be assembled for size-selective aerobic alcohol oxidation.[49] The components within the PCN-700 pores can function synergistically to achieve high size selectivity during catalytic conversions. Size-selective catalytic system can also be built in hierarchical core-shell MOFs. For instance, a series of functionalized core–shell MOFs, PCN-222(Fe)@Zr-NDC, PCN-222(Fe)@Zr-BPDC, and PCN-222(Fe)@Zr-AZDC (AZDC = azobenzene-4,4'-dicarboxylate) can be prepared with Fe-porphyrin moieties as core catalytic centers and isoreticular tunable UiO as shells for substrate selectivity control.[83] It was found that during olefin epoxidation, small olefins exhibited ideal conversions due to the high accessibility and activity of

the catalytic center. Importantly, the conversion decreases as olefin size increases, indicating the important role of the shell MOFs on limiting the diffusion rates of the substrates, and therefore the accessibility towards the catalytic centers. The tunable spatial environment around the catalytically active sites has also been realized in multicomponent MUF-77, where a catalytic unit in a pore is surrounded by linkers with different functional groups.[95] For example, prolinyl groups, catalytically active toward asymmetric aldol reactions, are placed in an identical environment, while installing functional groups on the linkers can systematically engineer the pore environment to alter the kinetic rates and the enantiomeric excess of the aldol products. These examples demonstrate the potentials of multi-component or hierarchical MOFs as tailored catalysts for heterogeneous reactions.

2.5.3 Guest Delivery

Because of the highly tunable pore environments inside of MTV-MOFs, guest transportation behavior can be highly controlled, allowing for a level of programmable guest release. Deng and coworkers reported a programmable release of guests by MTV-MIL-101, where three probe molecules, including ibuprofen, rhodamine B, and doxorubicin were systematically studied in a series of mesoporous MTV-MOFs with -H, $-NH_2$ and $-C_4H_4$ groups [MIL-101(Fe)-$(NH_2)_x$, MIL-101(Fe)-$(C_4H_4)_x$, and MIL-101(Fe)-$(C_4H_4)_x(NH_2)_{1-x}$] (**Figure 18c**).[22] The MTV-MOFs can adjust the rhodamine release rate by 32-fold [from MIL-101(Fe)-$(NH_2)_x$], and shift the doxorubicin release period from 12 days to 40 days [from MIL-101(Fe)-$(C_4H_4)_x(NH_2)_{1-x}$]. Importantly, the rate constants and the related molecular interactions were quantitatively correlated with the installed functionality mode and its ratio inside the MTV-MOFs, making predicted and programmed guest release possible. The concurrent release of two guests (RhB/Ibu and DOX/Ibu) in MIL-101(Fe)-$(NH_2)_x(C_4H_4)_{1-x}$ was also studied, with the results being consistent with the trends observed with single guest release. The controlled interactions between functional groups and guest molecules paves a way for the tailored pore environment of MTV-MOFs to be used for programmed drug release.

Hierarchical structures with various spatial distributions can couple functionalities into specific isolated domains in multicomponent structures, allowing them to function as a factory that can perform multitask production.[84] For example, PCN-223@MOF-177 was demonstrated as a designed hierarchical system with the ability to engage in phototriggered guest release. In this hierarchical structure, the shell MOF-177 has high porosity and guest storage capacity, while the core photoresponsive PCN-223 can be utilized to trigger the guest photothermal desorption. Remarkably, the phototriggered delivery of 4-nitrophenol was observed for the hierarchical PCN-223@MOF-177, demonstrating the efficient heat transfer from the core PCN-223 to the surrounding guest molecules absorbed in shells. These results exemplify the capability of multivariate hierarchical systems exhibiting cooperative behaviors to provide precise control over guest delivery and transportation.

2.5.4 Luminescence

Because of the presence of various tunable metal ions and organic linkers in their backbones, MOFs exhibit a wide range of luminescence characteristics. The Telfer group has shown that linker functionalization in MTV-MUF-77 can lead to the systematic tuning of the luminescence output (**Figure 18d**).[96] Interestingly, the emissive properties of MTV-MUF-77 can be well-controlled by linker modification, inter-linker energy transfer, and guest binding. The combination of a guanidine-based linker (yellow emitter, λ_{em} = 570 nm) and a strong blue emitter BDC-NH_2 (λ_{em} = 427 nm) into one framework can generate multicomponent MOFs as fluorescent materials with special spectral characteristics. Tunability of the metal clusters in multivariate or hierarchical MOFs can also enhance their domain- or orientation-controlled luminescence coding capabilities. For example, Su and coworkers prepared a series of core–shell heterometallic MOFs via liquid-phase epitaxial growth. The periodic organization of metal cluster are maintained while they exhibit structures with various spatial distributions.[97] The precise engineering of the positions of rare-earth elements opens a new route towards applications such as encoding, miniaturized displays, and other related areas.

3 Engineering Heterarchy and Hierarchy in COFs

Covalent organic frameworks (COFs), crystalline porous 2D or 3D polymers connected through reversible organic bonds, have attracted great attention since their first synthesis in 2005.[98] Compared with amorphous porous organic polymers (POPs) or porous polymer networks (PPNs), COFs are differentiated by their sequential assembly as a consequence of their directionally ordered bonds. The periodic skeleton and ordered pores in COFs allows for concise structural characterization using techniques such as X-ray diffraction and transmission electron microscopy (TEM).[99-101] Due to the modularity of COFs, their topology and pore size can be predesigned by through monomer shape control, leading to tailorable free volume. In contrast with hybrid inorganic-organic porous materials like MOFs, COFs are usually composed of light elements like H, B, C, N, and O connected through covalent organic bonds, which result in lower densities, greater stabilities, as well as wider potential applications.

3.1 Design Principle and Properties of Multicomponent COFs

From a structural perspective, COFs can be separated into two units: knots and linkers. Knots are made up of vertex monomers which direct topology, while linkers are made of edge monomers which assist in determining pore size (**Fig. 20**). Most COFs are comprised of one knot type monomer and one

linker type monomer, simplified as [1+1], in which the sequential connection of knots and linkers controls the chemistry of the pore environment and assembly. One breakthrough in COF design was the introduction of multicomponent COFs, which are comprised of more than one type of knot or linker, simplified as [1+n] or [n+1] (n>1). Multicomponent COFs have several advantages over two-component COFs: First, multicomponent COFs have more diverse compositions and versatile structures, permitting the combination of multiple functionalities. Second, the periodic organization of different functional groups can result in cooperative effects, which can be utilized to enhance catalytic activity or impart unusual physical properties. Third, multicomponent COFs makes it possible to design tailorable pore shapes and anisotropic skeletons, enriching the geometric configurations available to COFs.

3.1.1 Synthesis of COFs with various linkers

There are several strategies currently available for the design of multicomponent COFs, perhaps the simplest of which is the direct one-pot synthesis approach of mixing two different linkers or knots during synthesis.[102] In this approach, obtaining a crystalline material typically requires that the lengths or sizes of the monomers should be nearly the same. Typically, this results in this method being used with two linkers or knots that vary only by having different side chain substitutions. Such a strategy can be utilized to tune the loading ratio of specific function groups, modify the pore environment, or introduce novel properties into the COF to improve its performance in various applications. However, the chaotic distribution that can result from such a process increases the barrier for obtaining an ordered spatial assembly with functional group synergy.

Aiming to design COFs with tunable pore shapes and novel topologies, Zhao and coworkers synthesized two imine-linked COFs with a kagome lattice by utilizing one knot consisting of 4,4′,4″,4‴- (ethene-1, 1,2,2-tetrayl)tetraaniline (ETTA) and two linkers of different lengths, such as a combination of terephthalaldehyde (TPA) and [1,1′-biphenyl]-4,4′-dicarbaldehyde (BPDA) or a combination of BPDA and [1,1′:4′,1″-terphenyl]-4,4″-dicarbaldehyde (TPDA). The two resultant COFs, SIOC-COF-1 and SIOC-COF-2, bear three types of ordered pores, however their overall crystallinity and porosity are quite low.[103] The Zhao group and the Jiang group developed a bifunctional-linker strategy to synthesize COFs connected through both imine and boronate bonds by using 4-formylphenyl boronic acid (FPBA) as a linker and two different knots, HHTP and 1,3,5-tris(4-aminophenyl)-benzene (TAPB). This strategy has shown efficacy for the design of diverse hexagonal or tetragonal COFs with high crystallinities and porosities.[104, 105] Recently, a similar bifunctional-knot strategy was reported utilizing one cruciform knot and two different linkers to obtain tetragonal COFs.[106] Moreover, the Jiang group also performed a systematic study into the synthesis of multicomponent COFs and a general strategy was found wherein COFs with anisotropic skeletons and unique pore shapes could be obtained through the condensation reaction of one knot and two or three linkers of different lengths ([1+2] and [1+3]). The diversity of this strategy was proven by 44 highly crystalline examples of three-component hexagonal COFs synthesized through the [1+2] method and 6 four-component COFs from the [1+3] method (**Figure 20**). This not

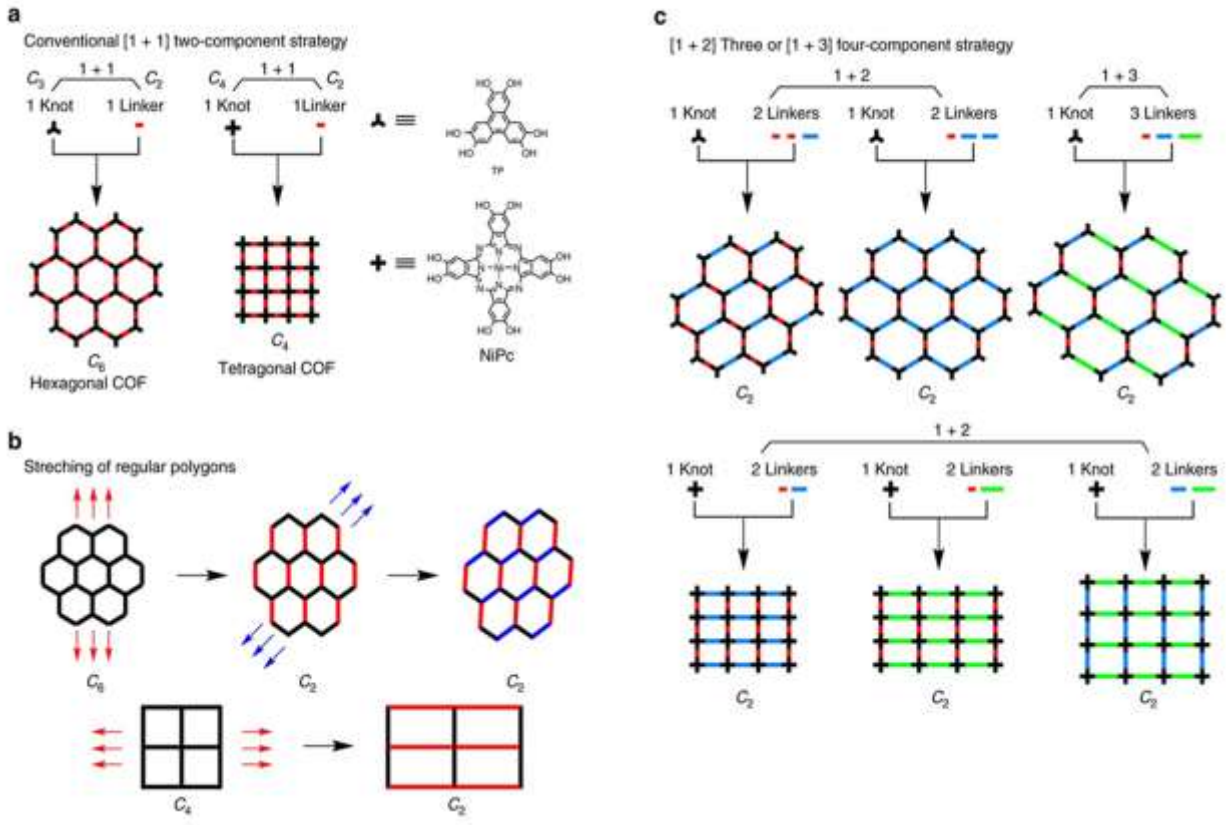

Figure 20. (a) Diagrams of the [1+1] strategy for 2D COF design using one knot and one linker. All the ligands are represented by bars with different colors. The topologies of the COFs depend on the symmetry of the knots, with a C_3-symmetric knot giving a hexagonal COF while a C_4-symmetric knot can form a tetragonal COF. (b) Installing linkers with various lengths will stretch the regular polygons of COFs. (c) Asymmetric tiling of multiple linkers to design [1+2] and [1+3] COFs with typical pore shapes. Reprinted with permission from ref. 107. Rights Managed by Nature Publishing Group.

only enriched the library of potential COF candidates, but also offered a novel method to boost the performance of COFs for application such as electric conductivity.[107]

3.1.2 Adsorption of multicomponent COFs

The structural diversity of multicomponent COFs has been improved through the incorporation of a wide variety of ligand structures, enabling the efficient design of new pore environments and skeletal geometries, allowing for synergistic improvements in physical and chemical properties. For instance, the Jiang group used novel linker designed for the systematic investigation of CO_2 uptake in a series of multicomponent porphyrin COFs.[108] Through a click reaction, they added various functional groups like hydroxy, amino, and carboxylic acid groups onto COF skeletons and tuned their loadings. Interestingly, the relationship between CO_2 adsorption capabilities and the polar group loading is not a linear, with only a moderate modification achieving maximum adsorbance. This observation was attributed to a balance between the two conflicting effects of decreasing porosity and boosted CO_2 affinity through the introduction of polar functional groups (**Figure 21**). In 2018, Zhu and coworkers observed a similar phenomenon in NH_3 adsorption of a COF modified with a carboxyl group.[109] They found that the NH_3 uptake reached a maximal amount when the loading of the carboxyl group was 17% and continuing to increase the carboxyl content would lead to a dramatic drop in the NH_3 adsorbing capacity. The loss of capacity was ascribed to a loss of accessible surface area and long-range order. Besides gas adsorption, multicomponent COFs have also shown improvement in liquid phase adsorption. Recently, the Dichtel group designed a series of amine-functionalized imine COFs to remove the common pollutants per- and polyfluorinated alkyl substances (PFAS) from water. They concluded that a COF with an amine loading of 28% could remove the largest amount of PFAS at the highest rate due to a synergistic effect between the improved affinity of the functional group and the hydrophobic pore surface.[110]

3.1.3 Asymmetric catalysis carried out by multicomponent COFs

The versatility of multicomponent COF makes them eligible platforms for some challenging applications such as asymmetric catalysis. In 2014, the Jiang group developed the first organocatalytic COF by integrating a pyrrolidine unit onto the edges of a tetragonal COF.[111] Although there was a kinetic preference introduced when tuning the loading of pyrrolidine, the enantio-selectivity (ee) was still low (around 50%). Later, the same group designed a highly-efficient chiral catalyst based on a ternary COF by incorporating (S)-pyrrolidine and methoxy groups onto the phenyl edges of a hexagonal COF. In this instance (S)-pyrrolidine worked as a catalytic site while the lone pairs on the methoxy groups could soften the interlayer repulsion to improve the stability and crystallinity of the COF.[112] Remarkably, the COF with a 17% substitution rate of (S)-pyrrolidine gave a yield of 95% and 92% ee when utilized for a 12 h Michael reaction, which was more rapid than analogues with a higher density of catalytic sites. This example demonstrates that large space between catalytic sites can contribute to efficiency of catalysts. In 2017, the Cui group attempted to append chiral groups onto knots of a hexagonal imine-linked COF and they found that the incorporation of chirality resulted in a decrease in the crystallinity and chemical stability of the COF. Due to this factor, they diluted the chiral

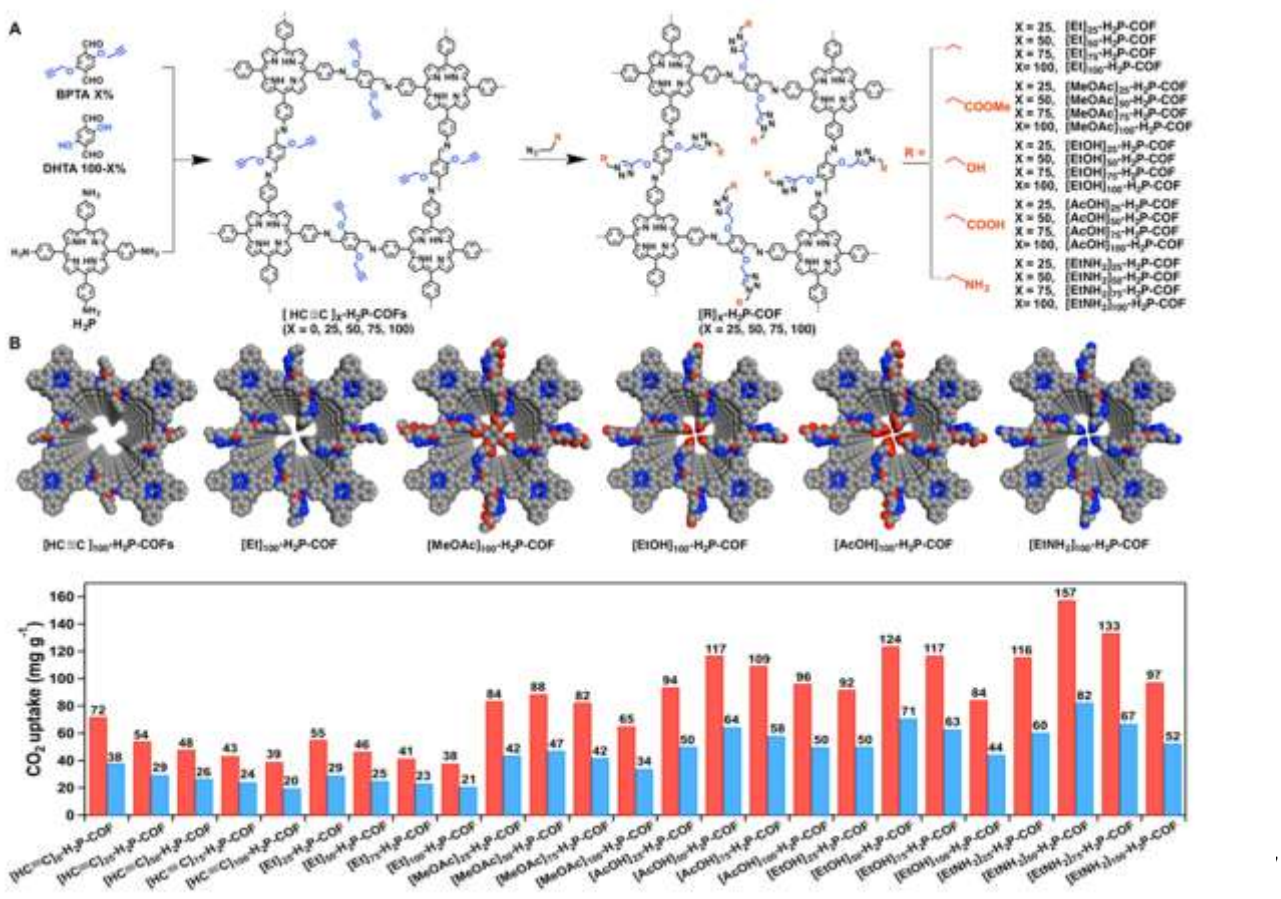

Figure 21. Installing various function groups onto COFs to achieve a synergistic boost in carbon dioxide adsorption. Reprinted with permission from ref. 108. Copyright©2015, American Chemical Society.

sites through co-condensation with achiral knots to obtain recyclable asymmetric catalysts that gave high yields and ee for three different asymmetric processes, the α-aminooxylation of aldehydes, as well as Aldol and Diels-Alder reactions.[113]

3.1.4 Multicomponent COFs as energy storage and photoelectric materials

High regularity and stability make COFs promising candidates for energy storage and photoelectric materials, However, finding strategies to improve the capacitance and conductivity of COFs remain challenging. Aiming to overcoming these barriers, multicomponent strategies have been adapted to improve the incorporation of useful properties within COFs. In 2014, the Jiang group reported three-component COFs working as donor-acceptor heterojunctions, in which electron-accepting fullerenes, C_{60}, were spatially confined in COFs with separated electron-donating nodes, with the efficiency of the photoinduced electron transfer and charge separation being tuned through the control of the density of the fullerene acceptors.[114] Recently, a corannulene integrated COF was reported by the Shustova group, which showed that packing of these π-bowls could promote conductivity in addition to donor-acceptor interaction.[115] Based on observations that the conductivity properties of COFs were not simply linear sums of their constituents, the Jiang group investigated the performance of ternary donor-acceptor COF systems, showing a nearly 1800 times improvement in conductivity.[107] To enhance the capacitance of COFs, the Jiang group utilized click reactions to immobilize redox-active TEMPO radicals onto a Ni-porphyrin COF.[116] Although the COF with a 100% loading of TEMPO gave a higher capacitance, the 50% loaded sample gave better retention of capacitance as well as a high-rate of ion transport, which was related to its high porosity. In 2018, Banerjee and coworkers fabricated β-ketoenamine-linker COFs based on anthracene linkers and redox-active anthraquinone linkers.[117] Through tuning the ratio of these two linkers, the redox activity and mechanical strength of the COF could be controlled.

3.2 Assemblies and Hierarchical Structures of COFs

The harmony of complexity and ordering in their structure allow COFs to be highly tunable materials with unique features that are useful for various applications. Akin to the multiple levels of protein structure, the architecture of COFs can be divided into three levels of hierarchy. The primary structure of a COF refers to the single layer or network as constructed by alternating monomers, this structure is bridged by covalent bonding and determines the chemical composition as well as basic structural skeleton of the COF. The secondary structure is formed through layer-by-layer packing or interpenetration of networks, driven by van der Waals, π-π stacking, hydrogen bonding, and other non-covalent interactions. The tertiary structure refers to the morphology of a COF, which can be sheeted, grained, hollowed, tubular and so on. Following the structure-property relationship, hierarchical COFs can be designed which will not only bring a greater deal of diversity and tunability to the material, but also integrate multiple properties and functions into their structures.

3.2.1 Stacking of two-dimensional COFs

For 2D COFs, the most common assembling pattern is stacking, which can be separated into three variations, eclipsed, staggered and slipped. The stacking pattern depends on the interactions between layers and the synthetic conditions. Numerous efforts have been devoted into improving stacking in order to obtain 2D COFs with higher crystallinity and porosity. Bein and coworkers designed monomers with propeller or armchair shapes as docking sites for synchronized stacking, which minimized the occurrence of stacking faults as well as dislocation and allowed for the formation of COFs with larger crystallite domain.[118, 119] The Jiang group reported an increase in COF crystallinity by self-complementary stacking of donors and acceptors,[120] and similar strategies like controlled layer arrangement through the alignment of dipole moments[112, 121] or hydrogen bonding.[122, 123] Recently, the Cui group succeeded in controlling interlayer stacking patterns through steric hinderance for a series of multicomponent COFs, in which COFs substituted with a higher number of alkyl groups tended to adapt AB or ABC stacking while those with less or smaller substituents preferred AA stacking.[124] Remarkably, the Cui group also incorporated chirality into their COFs through chiral induction, in which an asymmetric amine could impart chiral memory on the formation of single COF layers, resulting in the sequential assembly of a layered chiral crystallite.[125] Through control of the layer-by-layer sequence, many other interesting properties such as the J-aggregate of porphyrins[126] and layer-stacking-driven fluorescence[127] have been discovered in COFs.

3.2.2 Interpenetration of three-dimensional COFs

For 3D COFs, networks are mostly connected through interpenetration, with maximum of 11-fold interpenetration.[128] Through tuning synthetic conditions, COFs with different degrees of interpenetration can be synthesized.[129] Another unique manner of COF connection is weaving, first reported by the Yaghi group in 2016.[130] In Yaghi's work, they designed an interlaced monomer with a Cu(I) ion for templating and constructed the woven COF-505 through a condensation reaction. Interestingly, the demetallation of the Cu(I) ion led to looser interactions between threads and a ten-fold increase in elasticity. The special topology of woven COFs can trigger some distinct properties. For instance, woven COF-506 was able to take up guest molecule which exceeded its original pore size.[131] Such an adaptive guest inclusion can be attributed to the high flexibility of the weaving threads.

3.2.3 Self-assembly pathway to COFs with hierarchical morphology

Morphology is one of the key elements to determine the features and behaviors of COFs in practical application, which can be controlled spatially through self-assembly procedures.

For instance, in 2015, the Banerjee group reported a hollow spherical COF, DhaTab, with mesoporous walls for trypsin immobilization, with a mechanistic study being performed through analyzing COF samples after different reaction times.[132, 133] At early stages of the reaction COF crystallites would be assembled into coiled or dense spherical structures, and after 36 h hollow cavities appeared, indicating an inside-out Ostwald ripening process. In 2018, the Beuerle group synthesized a DPP-TAPP COF which could be spontaneously scrolled from sheet-like agglomerates to tubular microstructures.[134] The authors proposed that minimization of the destabilizing interactions with solvents led to the transformation, which was further supported by the similar thickness of the original sheet and the tubular wall.

The morphology of COFs can be affected by synthetic conditions. For example, in 2017 Trabolsi and coworkers discovered that solvent polarity and heating methods determined the fabrication modes of a viologen-linked COF, for which polar solvents would give a hollow spherical shape while nonpolar solvent would lead to hollow tubes.[135] In the same year, the Choi group developed a photochemical synthetic strategy for COF-5, in which UV irradiation accelerated the growth of COF-5 in the [001] direction dramatically, affording a 1D local morphology.[136] As a result, a hierarchical COF-5 with a sea-urchin-shape as well as an enlarged surface area was obtained, providing insights into the photochemical synthesis and patterned growth of COFs. In 2018, Horike and coworkers reported the construction of a hierarchical COF with defined core-shell domain via a postsynthetic approach.[35] It was found that either homogeneous or core-shell mixed-linker COFs could be obtained by controlling the reactivity of linkers. The resulting core-shell COFs had a 2-folder greater BET surface area and tunable hydrophilicity compared to the two parent phases.

3.2.4 Template-assisted pathway to COFs with hierarchal morphology

Moreover, hierarchal COFs can also be achieved through a template-assisted strategy. For instance, in 2015, the Banerjee group grew a chemically stable COF on the surface of ZnO nanorods to obtain hybrid materials.[137] Through acid treatment, a hollow COF with a capsule morphology could be achieved. In 2016, the Wang group manipulated COF hybrid microspheres with a photothermal conversion effect through the reconstruction of the imine bonds.[138] In this work, they first encapsulated Fe_3O_4 into an amorphous polyimine network, which could then be reformed into crystalline COFs *in situ*, allowing for uniform particle size, controllable COF shell thickness as well as magnetic responsiveness. In 2018, the Talyzin group realized the directed vertical growth of COF-1 onto graphene oxide (GO), wherein the boronic acid ligands would attach to the GO surface through covalent bonds, with the thickness of the COF-1 nanosheets being precisely controlled.[139] Recently, the Zhang group utilized polystyrene microspheres to fabricate hollow spherical porphyrin organic frameworks, whose polar chemical structures and hollow morphology showed the dual effects of chemical adsorption and physical confinement for mitigating the shuttle of polysulfides, making it a potential material for the sulfur cathode of lithium-sulfur batteries.[140]

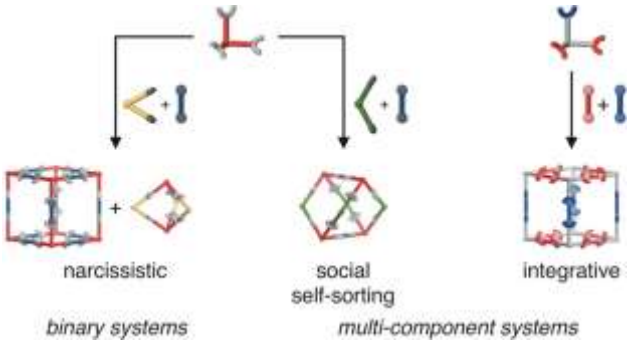

Figure 22. Two distinct binary cages can be obtained by mixing one knot and two ligands together through a narcissistic self-sorting, while a mixed-linker cage will be constructed through social or integrative self-sorting. Reprinted with permission from ref. 149. Copyright©WILEY-VCH Verlag GmbH & Co. KGaA, Weinheim.

4 Engineering Heterarchy and Hierarchy in Cage Compounds

Through elegant molecular fabrication, crystalline cage compounds with designable geometries and intrinsic porosities can be achieved. According to their compositions, cage compounds can be divided into two groups, metal-organic cages (MOCs) and porous organic cages (POCs). Driven by coordination self-assembly, MOCs, also dubbed metal-organic polyhedra (MOPs) or porous coordination cages (PCCs), are assembled from one or more types of ligands and metals, in which either the ligand or the metal node can work as a building block to determine the topology and geometry of the cage.[141-143] POCs are constructed from two or more organic synthons through covalent bonds, with the cage structures being highly dependent on the geometry of the synthons. Typically rigid linkers such as aryl groups or other highly conjugated molecules are utilized to maintain porosity after the removal of the synthesis solvents, as these linkers will minimize bond bending or rotation within the cage.[144-146] One interesting principle in the structural design of MOCs and POCs is the control over cage size through the tuning of the angles and length of ligands. Generally, a narrower angle will give a smaller cage while a wider angle will produce a larger one.[147] Additionally, both the intrinsic and extrinsic chemical environments of cage compounds can be modified through the immobilization of various functional groups, which can be arranged with great spatial precision. As such it is possible to combine multiple functions, guest recognition, catalysis, sensing, chirality, and photosensitizing within a cage compound to achieve complexity and synergy in a manner related to the active sites of proteins. The development of the methodologies for the synthesis of multicomponent cage

compounds not only results in the construction of structures with novel geometries, but also in structures with hybridized moieties with diverse chemical properties.

4.1 Self-sorting Strategy to Fabricate Heteroleptic MOCs

Heteroleptic strategies are usually utilized to synthesize multicomponent MOCs, however, a simple mixture of various ligands and metal ions can often lead to an intractable mixture. For example, the mixture of two different bis-monodentate ligands with Pd (II) ions can result in three possible outcomes. The first outcome results in the formation of two distinct homoleptic cages through narcissistic assembly, the second result forms a statistical mixture of heteroleptic cages, with the third result giving a pure phase of heteroleptic cages through integrative self-sorting (**Figure 22**).[148, 149] Remarkably, the integrative self-sorting strategy should be the most efficient pathway for the generation of desirable multifunctional MOCs without further purification, however it still requires rational design of the ligands and metal centers to properly control the self-assembly.

4.1.1 Templating synthesis of heteroleptic MOCs

The first strategy used for the fabrication of integrative heteroleptic MOCs is through the utilization of guest molecules as templates. In 2000, the Fujita group reported the effects of guest sizes on an equilibration between homoleptic and heteroleptic cages in the reaction of cis-protected Pd (II) ions and two tridentate pyridine ligands. They found that heteroleptic cages were preferred when adding guests of the appropriate sizes.[150] Later, the Fujita group discovered that planar aromatic guests could be applied to the assembly of cages with specific prism shapes.[151] In 2015, Yoshizawa and coworkers also reported the selective formation of a mixing-linker cage using fullerene C_{60} as a template.[152] However, if these situations, the cavity of the resulting cages are occupied by the template guests, restricting further modifications and potential applications.

4.1.2 Heteroleptic MOCs with complementary ligands

A second strategy for heteroleptic MOC construction is through the utilization of ligands with complementary shapes. In 2014, the Fujita group synthesized a cantellated tetrahedral cage $M_{12}(L^1)_{12}(L^2)_{12}$ by using Pd (II) ions and two bent dipyridyl ligands with different lengths.[153] (**Figure 23**) Interestingly, a larger difference in length will result in a well-defined icosahedral mixing linker cage compound. In 2016, the Clever group designed a hybridized bent cage, cis-$[Pd_2L^1{}_2L^2{}_2]$, based on an inward-bent acridone ligand and an outward phenanthrene ligand through a cage-to-cage transformation,[154] in which these two ligands matched with each other to achieve a bent shape. This strategy was further developed by introducing another outward-bent carbazole ligand.[155] Our group once performed a systematic study on the fabrication of multicomponent MOCs by partial substitution.[156] In this work, homoleptic cages were constructed with square four-connected $Cu_2(O_2CR)_4$ units and 1,3-benzenedicarboxylic acid analogues, which could be substituted by various dicarboxylic acids with longer backbones to precisely afford heteroleptic MOCs.

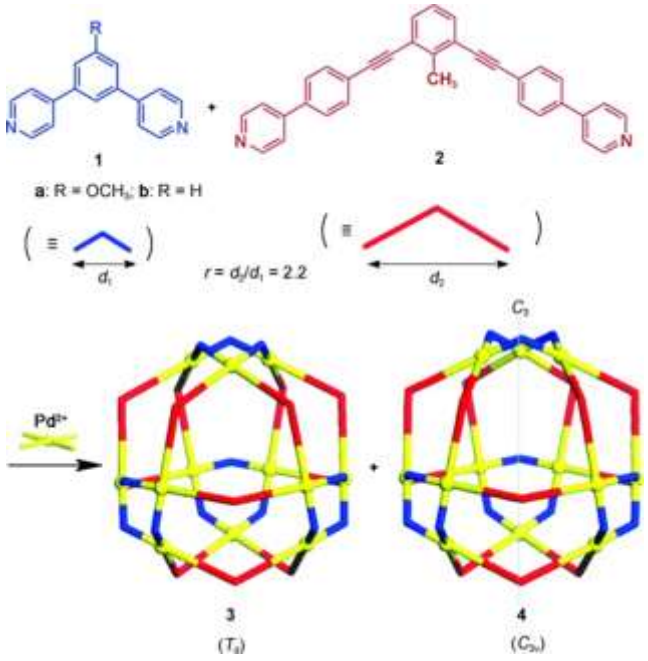

Figure 23. A strategy to obtain two different mixed-ligand MOPs by choosing bent ligands with different lengths. Reprinted with permission from ref. 153. Copyrignt©WILEY-VCH Verlag GmbH & Co. KGaA, Weinheim.

4.1.3 Multiple interaction guided assembly of heteroleptic MOCs

The third strategy is to introduce multiple interactions into the assembly process. For instance, the Hooley group utilized steric effects to control the self-sorting of a heteroleptic Pd (II) paddle-wheel cluster by adding bulky groups to the backbone of a bispyridine ligand.[157] Owing to space-filling interactions, the assembling pattern of the cage could be tuned through the size of the interior substituent. In 2016, Crowley and coworkers investigated the effects of intermolecular interactions on the heteroleptic assembly through introducing amine groups to the pyridyl ring of a banana-shaped tripyridyl ligand. They found a distinct heteroleptic cage could be selectively achieved because of hydrogen bonding and steric hindrance.[158] In 2010, the Stang group reported a series of multicomponent cages with trigonal or tetragonal prism geometries through mixing carboxylate and pyridyl ligands with cis-protected Pt (II) reagents, in which the Pt complexes had a lower energy when adopting a heteroleptic charge-separated pattern, which was further confirmed by a cage-to-cage transformation upon direct mixing of two homoleptic cages.[159]

4.2 Self-sorting Assembly of Multicomponent POCs

Self-sorting can also be observed in the fabrication of POCs, which are assembled through dynamic covalent chemistry (DCC) similar to COFs.[160, 161] As opposed to the metal-ligand interactions in MOCs, POCs are connected through reversible covalent bonds, allowing for more directional control on cage geometry and more selective bonding between different monomers. The Mukherjee group performed a systematic study of the narcissistic self-sorting of POCs. In 2012, the Mukherjee group discovered the narcissistic assembly of two triamines and two dialdehydes that resulted in only two binary cages out of four possible coordination modes, which could be driven by lessening of intramolecular stain. They dubbed this process molecular marriage since each monomer would only react with a specific counterpart.[162] Their subsequent work showed similar assembly driven cage formation through hydrogen bond interactions and geometric features induced control in nonsymmetric ligands.[163, 164] In 2015, the Beuerle group reported more complex structures based on boronic POCs using tritopic catechol-functionalized tribenzotriquinacene (TBTQ) and diboronic acids, which could be assembled through either narcissistic or social self-sorting, relying on the bite angles of the diboronic acids.[145] This was the first example of social self-sorting resulting in mixed linker POCs.

Moreover, multicomponent POCs with a statistical mixing of linkers can also result in novel properties such as altered solubility and adsorption. In 2011, the Cooper group presented a series of desymmetrized tetrahedral imine-linked POCs based on 1,3,5-triformylbenzene (TFB), 1,2-ethylenediamine (EDA) and (1R, 2R)-1,2-cyclohexanediamine (CHDA) ligands,[165] in which the as-synthesized cages had a scrambled distribution and contained intermolecular voids due to their weak packing interactions. The POCs also showed tunable but unpredictable gas selectivity behavior on H_2/N_2 by tuning the ratio of EDA and CHDA. Recently, Lively and coworkers designed defective imine-linked POCs by introducing isophthalaldehyde (IPA) into TFB and diaminocyclohexane (DACH), with the free amino group giving an increase in CO_2 uptake when incorporated into the cage.[166]

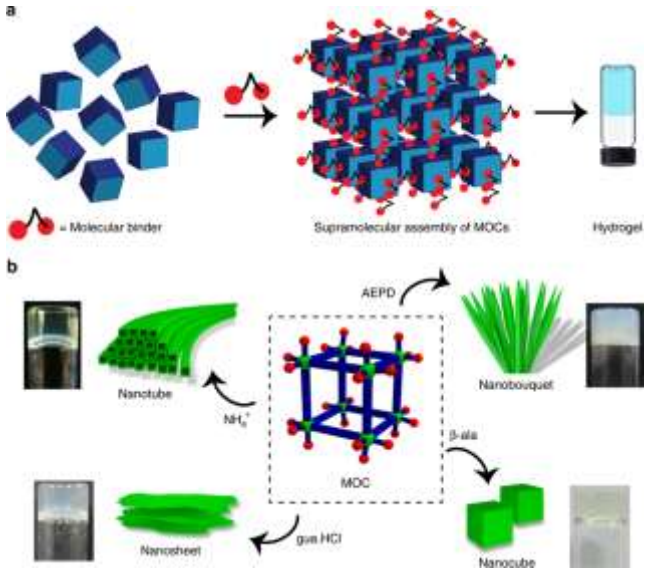

Figure 24. (a) Self-assembly of MOCs into hydrogels driven by molecular binders. (b) MOC-based superstructures with various morphologies achieved by using different molecular binders. Reprinted with permission from ref. 184. Rights Managed by Nature Publishing Group.

4.3 Hierarchical Assembly of MOCs and POCs

Owing to their peculiar topology, cage compounds can experience super-molecular assembly to form hierarchal structures. In general, there are two strategies to fabricate cage compounds together based on their connecting modes, interlocking and aggregation. Interlocking means that different cages interpenetrate mechanically with each other through entanglement with the cage cavity. Interlocking is affected by factors such as ligand shape, coordination environment, and the presence of solvent or guest molecules. Aggregation refers to the assembling of cages together, forming a super-molecular structure through intermolecular interactions located on the outer surface of the cage. Aggregation typically requires processes such as coordinative interactions or hydrogen bonding, and sometimes requiring chemical modification of the cage to be achieved. The molecular nature of cage compounds makes hybridization with other materials like polymers or gels straightforward, allowing for higher processability and better control over morphology.

4.3.1 Design of mechanically interlocked MOCs

Mechanically interlocked structures have been well developed in cage compounds especially for coordination cages with delicate structures such as catenanes,[167, 168] double trefoil knots,[169] and Borromean rings[170] having been reported to date. The interpenetration of MOCs are usually controlled through templating guests and bending angles and lengths of the ligands. Early in 1999, Fujita and coworkers reported the first molecular triply interpenetrated topology constructed through the self-assembly of two prism coordination cages bearing a quadruple aromatic stack.[171] To fabricate interpenetrated cages, bent or banana-shaped ligands are often utilized in concert with square-planar coordination metals such as Pd (II) and Pt (II). In 2008, the Kuroda group reported the first quadruply interpenetrated stranded cages by using Pd (II) ions and flexible banana-shaped dipyridyl ligands.[172] In 2012, Clever and coworkers attached pyridyl arms with various lengths onto dibenzosuberone to form rigid bent-shaped ligands. They discovered that the longer ligand could assemble with Pd (II) to produce interpenetrated cages with counterions, such as tetrafluoroborate, in their cavity.[173] Though introducing bulky groups to the backbone of the bent-shaped ligand, the interlock between two cages could be made tighter, enlarging the outer pocket space and allowing for the binding of larger anions such as ReO_4^-.[174] Additionally, the Clever group also found a system utilizing carbazole ligands

that could engage in the transformation from a double catenation to a triple catenation structure through the addition of halide ions.[175] In 2018, Clever and coworkers reported a large catenane which was comprised of two interlocked D_{4h}-symmetric Pd_4L_8 barrel-shaped cages.[176] This work was the result of a highly specific ligand bite angle, in this case a narrow angle of 60°, with this inward directed angle leading to the introverted assembly of cages.

4.3.2 Design of mechanically interlocked POCs

Devising three dimensional interlocking organic moieties has always been a challenge, however POCs, due to their rigid skeletons and internal cavities, exhibit high potential for interlocking. This system was not realized until 2010, when Cooper and coworkers reported the first example of multiply interlocked catenanes based on two tetrahedral imine-linked cages, which could be depicted as two interlocked 3-tori with six crossing cycles.[177] The dimers were synthesized by the acid-catalyzed condensation of triformylbenzene with three different diamines without the addition of exterior templates. In 2014, the Mastalerz group reported a quadruply interlocked boronic ester cage which exhibited a persistent shape and showed both defined micropores and mesopores, resulting in the first example of a porous molecular catenane.[178] In 2018, Cooper and coworkers performed a high-throughput screening of POCs through a combination of computational modeling and robotic synthesis.[179] This systematic study led to the discovery of a novel [8+12] cage with a doubly bridged triply interlocked catenane topology which was comprised of two different [4+6] cage units, confirming the advantage of experimental-computational workflow.

4.3.3 Non-interlocked MOC assemblies

Owing to their versatile exterior environments and multiple interaction sites, MOCs are promising building units for spatial organization into hierarchical structures through multiple interactions. In 2013, the Wei group reported what is potentially the first hierarchically assembled MOC network, produced from sulfonate-decorated MOCs into a three-dimensional porous network through metrically matched hydrogen bonding.[180] In 2015, Li and coworkers reported a mesoporous supramolecular framework with a diamond topology based on a Co-imidazolate MOC.[181] In this example, various anions work as nodes for bridging, with multiple interactions such as covalent bonds, dative bonds and weak hydrogen bonds being involved in the construction of the framework. The cages utilized in this studied were investigated for their use as molecular traps for molecules such as dyes and vitamin B_{12}. In the same year, Cheng and coworkers reported the controlled assembly of MOCs into two- or three-dimensional architectures driven by the formation of coordination bonds.[182] To achieve the polymerization of MOCs, they first synthesized MOCs with metal binding sites and phenolic ligands. The cages could crosslink through coordination bonds to afford hierarchal polymers, which showed a remarkable enhancement in gas adsorption compared with the cage monomers. In 2018, the Furukawa group manufactured a Rh-MOC monomer $[Rh_2(BDC)_2]_{12}$ into supramolecular polymers through crosslinking with ditopic imidazole-based linkers.[183] Interestingly, mechanistic studies indicated that the polymerization of the MOCs went through multiple stages, experiencing nucleation, elongation, and crosslinking. The macroscopic morphology of the supramolecular polymers could be tuned from spherical particles to gels with hierarchical porosity by controlling the amount of imidazole linker added. In the same year, Maji and coworkers reported hydrogels assembled from an anionic Ga-MOC $[Ga_8(ImDC)_{12}]_{12}^-$ cage and molecular binders driven by charge-assisted hydrogen bonding (**Figure 24**).[184] Remarkably, by choosing different types of molecular binders, namely the ammonium ions N-(2-aminoethyl)-1,3-propanediamine, guanidine hydrochloride, and β-alanine, the morphology of the hydrogels could be changed into nanotubes, nanobouquets, nanosheets, and nanocubes. Properties like luminescence could be introduced into the gels by adding a light harvesting antenna as a molecular binder. In 2016, the Johnson group prepared 'polyMOC' gels assembled from MOCs immobilized with polymetric ligands.[185] The high branch functionality of polyMOC gels resulted in rich loop defects, which could potentially be further replaced by functional groups like fluorescent groups while maintaining mechanical integrity. The structures of the polyMOC gels could be controlled by the shape and topology of the polymetric linkers.[186, 187] The Johnson group later installed photo-switchable ligands into the polyMOC gels to achieve the controllable rearrangement of the MOC junctions, affording networks with different topologies that showed great potential for fields such as soft robotics and photo-actuators.[188]

4.3.4 Non-interlocked assembly of POCs

The aggregation of POCs is intriguing owing to their spatial arrangement of functional group and permanent cavities. The Cooper group performed a systematic study on the controllable assembly of POCs by means of molecular recognition. In 2011, they reported the assembly of two chiral POCs through the utilization of a lock-and-key rule, which they used to achieve computationally predictable structures with tailorable pore volumes.[189] Such a strategy could also be extended to a three-component system they dubbed a porous organic alloy, in which a wide ratio of components could be used to give the reported first porous organic solid solution.[190] The Cooper group also attempted to introduce bulky groups which could interrupt the packing of POCs, leading to the coexistence of intrinsic and extrinsic pores.[191] In 2017, the same group constructed one-dimensional nanotubes and three-dimensional diamondoid networks based on pillared POCs, introducing reticular synthesis into molecular crystals.[192] Recently, core-shell crystals of POCs were fabricated through epitaxial growth by the sequential addition of distinct cage solutions, with a synergistic boost in CO_2 uptake and CO_2/CH_4 selectivity being observed in the hierarchal material.[193]

5 Hybrid Materials Constructed from MOFs, COFs, MOCs and POCs

As novel porous materials, MOFs, MOCs, COFs, and POCs have a number of structural similarities. The cage compounds possess intrinsic cavities as well as extrinsic skeletons, where the former allows for host-guest interactions and the latter results in persistent structures. Once bridged by extraneous junctions, those cages can be transformed into periodic frameworks with hierarchal porosity coming from both the cage cavities and the void spaces between cages. Moreover, both MOFs and COFs contain highly ordered skeletons and versatile function groups, which can be coupled by stepwise generation strategies.

5.1 Fabrication from Cages to Frameworks

One strategy used for the transformation of cages to frameworks is to introduce bridging agents, which could be organic ligands, ions, or even polymeric chains. The first hierarchal assembly going from MOCs to MOFs was reported by our group in 2009.[194] In this work, a cage compound, MOP-28 was synthesized with $Cu_2(CO_2)_4$ paddle-wheel clusters and 9H-carbazole-3,6-dicarboxylate (CD) ligands, where the Cu sites could be bridged by dipyridines to afford a cage-based MOF. In 2017, the Pan group crosslinked imine-based POCs together through the bridging of sodium ions, resulting in a hierarchal network with enhanced CO_2 uptake compared with its cage precursor.[195] Recently, the Kim group reported hierarchical assemblies of rigid porphyrin cages.[196] In this work, they first constructed cubic cages based on zinc-porphyrin units and they then bridged the cages through dipyridyl linkers to produce a framework with great potential for photocatalysis. Very recently, the Shimizu group crosslinked Cu_{24} isophthalate MOCs with long aliphatic chains.[197] Nanoindentation was applied to analyze the relationship between mechanical properties and crosslink densities, which demonstrated that a higher crosslink density could bring a boost in hardness while still retaining the MOC cavities. A similar strategy can be utilized for the fabrication of POCs into MOFs. In 2010, Cooper and coworkers reduced an imine-based cage into a cage with secondary amino groups, they then reacted the reduced cage with hexanuclear zinc carbonate clusters to afford a cage-MOF with organic pores.[198] Another strategy used for the synthesis of cage-based frameworks is to use trans-protected metal reagents. As mentioned above, cis-protected metals are often utilized as vertices to produce enclosed cage structures, while trans-protected metals can work as linear bridges to connect building units. For instance, in 2010, the Fujita group reported an infinite network coordination cage system based on 2,4,6-tris(4-pyridyl)-1,3,5-triazine (TPT) ligands and trans-$Co(NCS)_2$, which can not only work as a crystalline sponge for fullerenes but also gave a high selectivity for bimolecular reactions like acylation.[199, 200] In 2018, the Stang group reported a coordination cage assembled from tetra(4-(4-pyridinyl)phenyl)methane and bis[4,4'-(trans-$Pt(PEt_3)_2OTf$)]-diphenylmethanone.[201] The cages could be further connected by a linear reagent bis[1,4-(trans-$Pt(PEt_3)_2OTf$)] to form a diamondoid supramolecular coordination framework SCF-1. In 2018, Zhang and coworkers designed fluorescent organic cages based on tetrahydroxy-tetraphenylethylene and 2,3,5,6-tetrachloropyridine, and then connected these cages through Ni(0)-catalyzed Yamamoto-type Ullmann crosscoupling to produce networked cages.[202] Compared with their cage precursors, networked cages possessed an increase in porosity, owing to having overcome the window-to-arene packing of the free cages, and featured improved fluorescence response to CO_2.

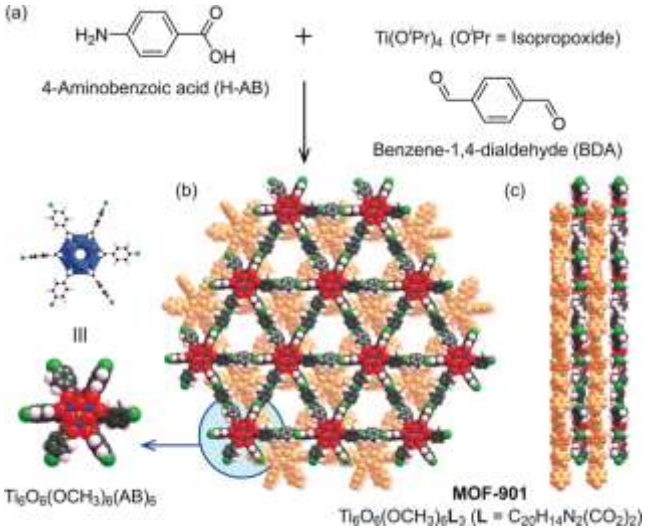

Figure 25. (a) A Ti(IV) oxo cluster was synthesized by condensation of 4-aminobenzoic acid (H-AB) and Ti(O^iPr)$_4$, which could be further connected by benzene-1,4-dialdehyde (BDA) to form MOF-901. (b) The structure of MOF-901 as viewed along the c-axis and (c) a-axis. Reprinted with permission from ref. 204. Copyright©2016, American Chemical

5.2 Hybrid Between MOFs and COFs

Though a combination of dynamic covalent chemistry and coordination chemistry, a hybridization of MOFs and COFs could be achieved through stepwise synthesis. In 2015, the Matzger group reported the introduction of reversible connections like imine bonds to control the topology of Zn-MOF.[203] In 2016, the Yaghi group reported the first combination of MOFs and COFs, in which hexameric Ti(IV) clusters were constructed and then connected through imine bonds to form MOF-901, which was an efficient photocatalyst for methyl methacrylate polymerization (**Fig. 25**).[204] In 2018, Lan and coworker anchored NH_2-UiO-66 onto TpPa-1-COF through imine bond formation.[205] The resulting MOF/COF hybrid material featured a tunable photocatalytic H_2 evolution rate by changing the MOF:COF ratio. In the same year, Zhang and coworker modified NH_2-MIL-68(In) with tris(4-formylphenyl)amine (TFPA), which sequentially served as a core for the reaction with tris(4-aminophenyl)amine (TAPA) to grow TPA-COF as shell to afford a core-shell hybrid material.[206] A similar strategy was also reported by the Kim group, who constructed a Pd doped MOF@COF core-shell hybrid through

the interfacial growth of LZU-1 onto amino functionalized MIL-125 (Ti).[207]

Summary and Outlook

With increasing requirements for multifunctionalities and hierarchical structures in various applications, the study of multi-component hierarchical MOFs and other open framework compounds have prospered in recent years. Extensive efforts have been made to develop synthetic strategies for multi-component hierarchical MOFs with tunable linker or metal compositions and distributions, to decrypt the apportionment of these building blocks insides functional materials, and to utilize the cooperative effects among the multiple components and domains for specific applications. The one-pot or post-synthetic preparation of multi-component MOFs with tunable apportionment can be achieved, which allows us to fabricate sophisticated structures with synergic effects. Investigating the local pore environments insides multi-component hierarchical MOFs is critical to enhancing our understanding of the "structure-property-application" relationship, which shall guide the state-of-art design and synthesis of well-controlled porous materials. However, current characterization methods are still limited, lagging far behind the level of characterization seen in the biological systems, such as protein and DNA, that MTV-MOFs are attempting to imitate. In this respect, more systematic and precise characterization procedures are required to obtain more information in the local pore environment of multi-component hierarchical framework compounds. Based on currently utilized techniques discussed above, the current batch of MTV-MOFs have shown wide applications including gas storage, separation, heterogeneous catalysis, guest delivery and luminescence behavior, exhibiting unexpected advantages over conventional single-component materials. MTV-MOFs can also serve as precursors for the preparation of other advanced functional materials including hierarchically porous structures, which also provides new routes to tune the porosity and functions of the resulting materials.

Programable pore environments have made major progress in the past decade. With growing research interests in multi-component hierarchical materials, an increasing number of related compounds have been reported, which show great applications in the area of selective binding and cooperative processes. However, the diversity and hierarchy of these materials have yet to reach the level of similarly complex biomaterials such as proteins and DNAs. From a synthetic perspective, future investigations should involve the "total synthesis" of complex frameworks from simple, basic building units through sequential chemical steps. The synthetic methodology in inorganic chemistry based on coordination bonds should be systematically designed and developed in the future. Additionally, the detailed characterization on the local porous environment, as well as their broader commercial and industrial scale applicability still need to be addressed. Despite the existing challenges in the development of both multi-component and hierarchical materials, advances in both new synthetic methodologies and characterization methods will continue to accelerate the discovery of multi-component hierarchical porous materials. When considering the high designability and diversity of these structures, it is easy to imagine a coming era filled by smart materials with unlimited tunability, synergism, and precision.

Conflicts of interest

There are no conflicts to declare.

Acknowledgements

This work was supported by the Center for Gas Separations, an Energy Frontier Research Center funded by the U.S. Department of Energy, Office of Science, Office of Basic Energy Sciences under Award Number DE-SC0001015, the Robert A. Welch Foundation through a Welch Endowed Chair to HJZ (A-0030), U.S. Department of Energy Office of Fossil Energy, National Energy Technology Laboratory (DE-FE0026472) and National Science Foundation Small Business Innovation Research (NSF-SBIR) under Grant No. 1632486. The authors also acknowledge the financial supports from the Qatar National Research Fund under Award Number NPRP9-377-1-080.

Table 1 Summary of some representative multi-component MOFs and their applications.

Name	Component I[a]	Component II	Component III	Applications	Ref.
Mixed-linker MOFs					
UiO-66-TCPP	BDC	TCPP	BDC-NH_2, etc.	Biomimetic catalysis	25
PCN-900 (RE)	TCPP	BPDC	-	CO_2 conversion	35
MTV-MOF-5 (Zn)	BDC	BDC-NH_2	BDC-NO_2, etc.	CO_2/CO separation	19
MTV-MOF-177 (Zn)	BTB	BTB-NH_2	BTB-NO_2, etc.	Gas storage	20
Pt⊂UiO-66-S,N	BDC-SO_3H	BDC-NH_2	Pt	Gas-phase catalysis	21
MTV-MIL-101	BDC	BDC-NH_2	NDC	Drug delivery	22
MTV-Zn[M(salen)]	Cu(salen)	V(salen)	Mn(salen), etc.	Sequential asymmetric catalysis	26
MTV-Zr[M(salen)]	Cu(salen)	V(salen)	Mn(salen), etc.	Sequential asymmetric catalysis	27
UMCM-1 (Zn)	BDC	BTB	-	-	26
ST-1 (Zn)	BDC	TATAB	-	Methane storage	29
CPM-12 (In)	BTC	BTB	-	Gas separation	31
CPM-33 (Ni)	BDC	TPT	-	Gas storage	32
MTV-ZIF-series (412)	IM	bIM	nIM	Volatile organic compound removal	33
PCN-134 (Zr)	BTB	TCPP	-	Photocatalytic degradation	34
sph-MOF-1 (RE)	TIA	BTCB	-	-	36
PCN-700 (Zr) series	BDC	BPDC-Me_2	TPDC	Size selective catalysis	49
PCN-609 (Zr)	CBTB	BDC	BPDC & TPDC	-	53
PCN-201 (Zr)	TCPP	Ni(INA)$_2$	-	Cooperative bimetallic catalysis	54
MUF-7 (Zn)	BDC	BPDC	BTB	CO_2 storage	94
MUF-77 (Zn)	BDC	BPDC	BTB	Asymmetric catalysis	95
Mixed-metal MOFs					
MTV-MOF-74	Mg	Co	Ni, Zn, etc.	-	55
$(M_3O)_2$(TCPP-M)$_3$	Mn	Fe	Co, Mg, etc.	Photocatalysis	56
PCN-415	Ti	Zr	-	Photocatalytic hydrogen evolution	64
PCN-800 (Zr)	Zr	Ni	Co, In, etc.	Acetaldehyde cyclization	67
NU-1000-Co	Zr	Co	-	Oxidative dehydrogenation of propane	68
PCN-160-$NiCl_2$	Zr	Ni	-	Ethylene dimerization	71
PCN-161-$CoCl_2$	Zr	Co	-	Magnetic relaxation	72

Table 1 Summary of some representative multi-component MOFs and their applications.

Name	Component I[a]	Component II	Component III	Applications	Ref.
Hierarchical Structures					
PCN-222@UiO-67	Zr/TCPP	Zr/BPDC	-	Size-selective catalysis	83
$[Zn_2(NDC)_2(DABCO)]_n$	NDC	DABCO	-	-	72
MOF-5-NH_2@MOF-5	Zn/BDC-NH_2	Zn/BDC	-	-	75
Bio-MOF-14@11	Co/	Co/	-	Selective CO_2 capture	76
MIL-68@MOF-NDC	In/BDC	In/NDC	-	-	77
ZIF-67@ZIF-8	Co/mIM	Zn/mIM	-	-	77
(ZIFs@)$_{n-1}$ZIFs	Co/mIM	Zn/mIM	Co/mIM, etc.	Hydrogen spillover	80
UiO-66-NH_2@MIL-125	Zr/BDC-NH_2	Ti/BDC	-	Photocatalytic degradation	82
PCN-222@MOF-5	Zr/TCPP	Zn/BDC	-	-	84
PCN-222@ZIF-8	Zr/TCPP	Zn/mIM	-	Phototriggered guest release	84

[a] Ligands are abbreviated as: BDC = terephthalate; BDC-NH_2 = 2-aminoterephthalate; TCPP = meso-tetrakis(4-carboxylatephenyl)porphyrin; BPDC = biphenyl-4,4'-dicarboxylate; NDC = naphthalene-2,6-dicarboxylate; BTC = benzene-1,3,5-tricarboxylate; BTB = 1,3,5-benzenetrisbenzoate; TPDC = [1,1':4',1"-terphenyl]-4,4"-dicarboxylate; TATAB = 4,4',4''-s-triazine-1,3,5-triyltri-p-aminobenzoate; BTCB = 4,4',4''-((benzene-1,3,5-tricarbonyl)tris(azanediyl))tribenzote; CBTB = 4,4',4",4"'-(9H-carbazole-1,3,6,8-tetrayl)tetrabenzoate; INA = isonicotinate; mIM = 2-methylimidazolate; bIM = benzimidazolate; nIM = 2-nitroimidazolate.

Table 2 Summary of some representative heterarchical/hierarchical COFs and their applications.[a]

Name	Component I[a]	Component II	Component III	Applications	Ref.
Multicomponent COFs					
X%N_3-COF-5	HHTP	BDBA	N_3-BDBA, etc.	-	102
SIOC-COF-1	ETTA	TPA	BPDA	-	103
SIOC-COF-2	ETTA	BPDA	TPDA	-	103
NTU-COF-2	TAPB	HHTP	FPBA	-	104, 105
Aniso-COFs	BAAT	BDBA, etc.	TPA, etc.	-	106
MC-COF-series	HHTP	BTDADA, etc.	TTDA, etc.	Conductivity	107
[R]$_x$-H_2P-COF	H_2P	DHTA	BPTA, etc.	CO_2 adsorption	108
[HOOC]x-COF	TFP	DAA	PEA	Ammonia capture	109
X%[NH_2]-COF	TAPB	TPA	NH_2-TPA, etc.	Polyfluorinated alkyl substance (PFAS) removal	110
[(S)-Py]$_x$-TPB-DMTP-COFs	TAPB	DMTA	(S)-Py-TPA	Chiral catalysis	112
CCOF-DMTA-TPB	TAPB	L-Pro-TAPB, etc.	DMTA	Chiral catalysis	113
[C_{60}]$_x$-ZnPc-COF	ZnPc[OH]$_8$	BDBA	C_{60}-BDBA	Photoinduced electron transfer	114
[πB]-COF	TAPB	DMTA	πB-TPA	Conductivity	115
[TEMPO]$_x$-NiP-COF	NiP	DMTA	TEMPO-TPA	Capacitive energy storage	116
DqDaTp-COF	TFP	Da	Dq	Flexible supercapacitor electrode	117

Name	Component I[b]	Component II	Morphology	Applications	Ref.
Hierarchical COFs					
COF-505	Cu(PDB)$_2$(BF_4)	BZ	Weaving	Dye adaptive inclusion	130, 131
COF-DhaTab	Tab	Dha	Hollow sphere	Enzyme adsorption	145
CPP-2,3-DhaTta	Tta	2,3-Dha	Ribbon	-	146
DPP-TAPP-COF	TAPP	DPP-1	Microtube	-	134
Viologen-COF	TAPB	BDB	Hollow sphere and tube	Iodine adsorption	135
UV-COF-5	HHTP	BDBA	Sea urchin shape	-	136
COF-Naph-Ph	TFB/Ph	TFB/Naph	Core-shell	Water sorption	35
Fe_3O_4@COF(TpBD)	TFP	BZ	Core-shell	Photothermal effect	138
v-COF-GO	BDBA	GO	Vertical sheet	Supercapacitor electrode	139

[a] Ligands are abbreviated as: HHTP = hexahydroxytriphenylene; BDBA = benzenediboronic acid; N_3-BDBA = azide-appended benzenediboronic acid; ETTA = 4,4′,4″,4‴-(ethene-1, 1,2,2-tetrayl)tetraaniline; TPA = terephthalaldehyde; BPDA = [1,1′-biphenyl]-4,4′-dicarbaldehyde; TPDA = [1,1′:4′,1″-terphenyl]-4,4″-dicarbaldehyde; TAPB = 1,3,5-tris(4-aminophenyl)-benzene; BAAT = 9,10-bis(4-aminophenyl)-anthracene-2,3,6,7-tetraol; BTDADA = 1,4-benzothiadiazole diboronic acid; TTDA = thieno[3,2-b]thiophene-2,5-diyldiboronic acid; H_2P = 5,10,15,20-tetrakis(p-tetraphenylamino)porphyrin; DHTA = 2,5-dihydroxyterephthalaldehyde; BPTA = 2,5-bis(2-propynyloxy) terephthalaldehyde; TFP = triformylphloroglucinol; DAA = 2,5-diaminobenzoic acid; PEA = p-phenylenediamine; NH_2-TPA = amino-appended terephthalaldehyde; DMTA = 2,5-dimethoxyterephthalaldehyde; (S)-Py-TPA = (S)-pyrrolidine appended terephthalaldehyde; L-Pro-TAPB = L-proline-1,3,5-tris(4-aminophenyl)-benzene; ZnPc[OH]$_8$ = (2,3,9,10,16,17,23,24-octahydroxyphthalocyaninato)zinc; C_{60}-BDBA = C_{60}-appended benzenediboronic acid; πB-TPA = corannulene-appended terephthalaldehyde; NiP = nickel 5,10,15,20-tetrakis(4’-tetraphenylamino) porphyrin; TEMPO-TPA = TEMPO-appended terephthalaldehyde; Da = 2,6-diaminoanthracene; Dq = 2,6-diaminoanthraquinone.

[b] Ligands are abbreviated as: Cu(PDB)$_2$(BF_4) = Cu(I)-bis[4,4'- (1,10-phenanthroline-2,9-diyl)dibenzaldehyde]; BZ = benzidine; Tab = 1,3,5-tris(4-aminophenyl)benzene; Dha = 2,5-dihydroxyterephthalaldehyde; 2,3-Dha = 2,3-dihydroxyterephthalaldehyde; Tta = 4,4',4"-(1,3,5-triazine-2,4,6-triyl)trianiline; TAPP = 5,10,15,20-tetrakis(4-aminophenyl)porphyrin; DPP-1 = 5,5’-(2,5-bis(2-ethylhexyl)-3,6-dioxo-2,3,5,6-tetrahydropyrrolo[3,4-c]pyrrole-1,4-diyl)dithiophene-2-carbaldehyde; TAPB = 1,3,5-tris(4-aminophenyl)-benzene; BDB = 1,1′-bis(2,4-dinitrophenyl)-[4,4′-bipyridine]-1,1′-diium dichloride; HHTP = hexahydroxytriphenylene; BDBA = benzenediboronic acid; TFB = 1,3,5-triformylbenzene; Ph = 1,4-diaminobenzene; Naph = 1,4-diaminonaphthalene; GO = graphene oxide.

Table 3 Summary of some representative heterarchical/hierarchical cages and their applications.

Name	Component I[a]	Component II	Component III	Applications	Ref.
Heteroleptic MOCs					
Heteroleptic cage (Pd)	$Pd(en)(NO_3)_2$	TPMB	DPMPB	-	150
Pyrazine-pillared cage (Pt)	$Pt(en)(NO_3)_2$	TPTZ	PZ	-	151
Cantellated tetrahedron (Pd)	$Pd(BF_4)_2$	DPB, etc.	PPEMB	-	153
Bent cage (Pd)	$[Pd(CH_3CN)_4](BF_4)_2$	DIQEHA, etc.	DPDMP, etc.	-	154, 155
Mix-linker MOP (Cu)	$Cu_2(OAc)_4 \cdot H_2O$	5-t-Bu-1,3-BDC, etc.	3,3'-EDDB, etc.	-	156
$[Pd_2(tripy)_2(2A\text{-}tripy)_2]$	$Pd(NO_3)_2$	tripy	2A-tripy, etc.	-	158
Charge separated cage (Pt)	$cis\text{-}Pt(PEt_3)_2(OTf)_2$	Na_2-BDC	BPEB	-	159
Multicomponent POCs					
$(TBTQ)_4(MTDA)_4(t\text{-}Bu\text{-}BDBA)_2$	TBTQ	MTDA	t-Bu-BDBA, etc.	-	144-146
Desymmetric POCs	TFB	EDA	CHDA	H_2/N_2 separation	165
Defective POCs	TFB	IPA	DACH	CO_2 adsorption	166

Name	Component I[b]	Component II	Assembly	Applications	Ref.
Hierarchical MOCs					
Triply interlocked cages (Pd/Pt)	$Pt(en)(NO_3)_2$, etc.	TPTZ/TPMPT	Interlock	-	171
Quadruply interlocked cages (Pd)	$Pd(NO_3)_2$	PMOBP	Interlock	-	172
Sardine-packing interlocked cages (Pd)	$[Pd(CH_3CN)_4](BF_4)_2$	BPEHBA, etc.	Interlock	Selective anion adsorption like ReO_4^-	173, 174
Networked GS MOCs	$Cu_2(OAc)_4$	Na-S/G	Network	Cationic dye adsorption	180
Networked imine-linked MOCs	$Co(ClO_4)_2 \cdot 6\ H_2O$	MFI/XEDA	Network	Dye and vitamin adsorption	181
Coordination-driven MOC polymer	$Cu_2(OAc)_4 \cdot H_2O$	H_2(5-OH-1,3-BDC)	Network	Gas adsorption	182
Ditopic-linker MOP polymer	$[Rh_2(OAc)_4]$/biz	bix	Crosslink	-	183
MOC-Gx hydrogel	$Ga(NO_3)_3 \cdot 6H_2O$/ H_3ImDC	NH_4^+, AEPD, gua.HCl or β-ala	Tube, bouquet, sheet or cube	Luminescence, dye adsorption	184
polyMOC gels	$Pd(NO_3)_2 \cdot 2H_2O$	PL1 or PL2	Twine polymer gel	Fluorescence, photo-actuator	185,188
Hierarchical POCs					
Triply interlocked POCs	TFB	PDA, etc.	Interlock	-	177
Quadruply interlocked [12+8] cages	BTBA	TTTO, etc.	Interlock	-	178
Bridged cage catenane [8+12]	TMB/DMTA	TMBTMA/ DMTA	Interlock	-	179
Cocrystal of R/S POCs [4+6]	TFB/S-CPDA, etc.	TFB/R-CHDA, etc.	Packing	-	189-191
TCCx [3+6]	TPTCD, etc.	R-CHDA	Packing	-	192
Core-shell POCs [4+6]	TFB/R-CHDA	TFB/S-CHDA	Core-shell	CO_2/CH_4 seperation	193

Table 4 Summary of hybridization of MOFs, COFs, and cages and their applications.

Name	Component I[a]	Component II	Component III	Applications	Ref.
From cages to frameworks					
MOP-28	$Cu(NO_3)_2{\cdot}2.5H_2O$	CD	DP	-	194
Imine-linked NC	TFBPD	DACH	Na^+	CO_2 adsorption	195
PSS	Zn-PB	DPB		Photo-catalysis	196
MOPx80	$Cu(NO_3)_2{\cdot}2.5H_2O$	m-BDC	OOIPA	-	197
[4+6]-cage MOF	$Zn(NO_3)_2{\cdot}6H_2O$	TFB	EDA	-	198
M_6L_4-cage framework	trans-$Co(NCS)_2$	TPT		Fullerene adsorption	198,213
SCF-1	BTDPM-Pt	TPPM	BT-Pt	-	201
pTOC	THTPE	TCP		CO_2 fluorescent response	202
Hybrid between MOFs and COFs					
UMCM-306	$Zn(NO_3)_2{\cdot}6H_2O$	NH_2-BTB	TPA	-	203
MOF-901	$Ti(O^iPr)_4$	AB	BDA	Photocatalyzed polymerization	204
NH_2-Uio-66/TpPa-1-COF	NH_2-Uio-66	TpPa-1-COF		Photocatalyzed H_2 evolution	205
NH_2-MIL-68@TPA-COF	NH_2-MIL-68 (In)	TFPA		Photocatalyzed degradation of rhodamine B	206
Pd/TiATA@LZU1	Ti/H_2ATA	TFB	PDA	Photocatalyzed dehydrogenation	207

[a] Ligands are abbreviated as: CD = 9H-carbazole-3,6-dicarboxylate; DP = dipyridine; TFBPD = 3,3′,5,5′- tetraformyl-4,4′- biphenyldiol; DACH = (1*R*,2*R*)/(1*S*,2*S*)- 1,2- diaminocyclohexane; Zn-PB = zinc-metalated porphyrin box; DPB = 1,4-di(4-pyridyl)benzene; m-BDC = 1,3-benzenedicarboxylate; OOIPA = 5-(octyloxy)isophthalic acid; TFB = 1,3,5-triformylbenzene; EDA = 1,2-ethylenediamine; TPT = 2,4,6-tris(4-pyridyl)-1,3,5-triazine; TPT = 2,4,6-tris(4-pyridyl)-1,3,5-triazine; BTDPM-Pt = bis[4,4'-(trans-Pt(PEt_3)$_2$OTf)]-diphenylmethanone; TPPM = tetra(4-(4-pyridinyl)phenyl)methane; BT-Pt = bis[1,4-(trans-Pt(PEt_3)$_2$OTf)]; THTPE = tetrahydroxy-tetraphenylethylene; TCP = 2,3,5,6-tetrachloropyridine; NH_2-BTB = 2,4,6- tris(4- carboxyphenyl)aniline; TPA = terepthalaldehyde; AB = 4-aminobenzoate; BDA = benzene-1,4-dialdehyde; TFPA = tris(4- formylphenyl)amine; H_2ATA = 2-aminoterephthalate; PDA = p-phenylenediamine

[a] Ligands are abbreviated as: en = ethylenediamine; TPMB = 1,3,5-tris(4-pyridylmethyl)benzene; DPMPB = 1,5-di(4-pyridylmethyl)-3-pyridylbenzene; TPTZ = 2,4,6-tri(4-pyridyl)-1,3,5-triazine; PZ = pyrazine; DPB = 1,3-di(4-pyridyl)benzene; PPEMB = 1,3-[2-(4-pyridinyl-4-phenyl)ethynyl]-2-methylbenzene; DIQEHA = 2,7-di[2-(8'-isoquinoline)ethynyl]-10-hexylacridin-9(10H)-one; DPDMP = 3,6-di(4-pyridyl)-9,10-dimethoxyphenanthrene; 5-t-Bu-1,3-BDC = 5-t-butyl-1,3-benzenedicarboxylic acid; 3,3'-EDDB = 3,3′-(ethyne-1,2-diyl)dibenzoic acid; tripy = tripyridyl; 2A-tripyridyl = 2-amino-substituted tripyridyl; Na_2-BDC = disodium 1,4-benzenedicarboxylate; BPEB = 1,4-bis(pyridine-4-ylethynyl)benzene; TBTQ = catechol- functionalized tribenzotriquinacene; MTDA = 2'-methyl-[1,1':3',1''-terphenyl]-4,4'-diboronic acid; t-Bu-BDBA = 2,5-di-t-butyl-1,4-benzenediboronic acid; TFB =1,3,5-triformylbenzene; EDA = 1,2-ethylenediamine; CHDA = (1R, 2R)-1,2-cyclohexanediamine; IPA = isophthalaldehyde; DACH = diaminocyclohexane.

[b] Ligands are abbreviated as: en = ethylenediamine; TPTZ = 2,4,6-tri(4-pyridyl)-1,3,5-triazine; TPMPT = 2,4,6-tris[4-(pyridin-4-ylmethyl)phenyl]-1,3,5-triazine; PMOBP = 4,4'-(3-pyridinemethoxy)benzophenone; BPEHBA = 3,7-bis(pyridin-3-ylethynyl)-10,11-dihydro-5H-dibenzo[a,d][7]annulen-5-one; G = guanidium; Na-S = sodium 5-sulfoisophthalate; MFI = 5-methyl- 4- formylimidazole; XEDA = *m*- xylylenediamine; H_2(5-OH-1,3-BDC) = 5-hydroxy-1,3-benzenedicarboxylic acid; biz = 1-benzylimidazole; bix = 1,4-bis(imidazol-1-ylmethyl)benzene; H_3ImDC = 4,5-imidazoledicarboxylic acid; AEPD = N-(2-aminoethyl)-1,3-propanediamine; gua.HCl = guanidine hydrochloride; β-ala = β-alanine; PL1 = para-bispyridyl appended PEG; PL2 = meta-bispyridyl appended PEG; TFB = triformylbenzene; PDA = propane-1,2-diamine; BTBA = benzene tris(boronicacid); TTTO = triptycene tetraol; TAMB = 1,3,5-tris(aminomethyl)benzene; TMBTMA = (2,4,6- trimethylbenzene-1,3,5-triyl)trimethanamine; DMTA = 2,5-dimethoxyterephthalaldehyde; S-CPDA = (1S,2S)-cyclopentanediamine; R-CHDA = (1R,2R)-cyclohexanediamine; TPTCD = [1,1':4',1''-terphenyl]-3,3'',5,5''-tetracarbaldehyde; S-CHDA = (1S,2S)-cyclohexanediamine.

Reference

1. M. J. Allen, V. C. Tung and R. B. Kaner, *Chem. Rev.*, 2010, **110**, 132-145.
2. Z. X. Li, J. C. Barnes, A. Bosoy, J. F. Stoddart and J. I. Zink, *Chem. Soc. Rev.*, 2012, **41**, 2590-2605.
3. I. Manners, *Angew. Chem. Int. Ed.*, 1996, **35**, 1602-1621.
4. J. Perez-Ramirez, C. H. Christensen, K. Egeblad, C. H. Christensen and J. C. Groen, *Chem. Soc. Rev.*, 2008, **37**, 2530-2542.
5. J. F. Lutz, M. Ouchi, D. R. Liu and M. Sawamoto, *Science*, 2013, **341**, 628-+.
6. S. Yuan, L. Feng, K. Wang, J. Pang, M. Bosch, C. Lollar, Y. Sun, J. Qin, X. Yang, P. Zhang, Q. Wang, L. Zou, Y. Zhang, L. Zhang, Y. Fang, J. Li and H. C. Zhou, *Adv. Mater.*, 2018, DOI: 10.1002/adma.201704303.
7. J. R. Li, J. Sculley and H. C. Zhou, *Chem. Rev.*, 2012, **112**, 869-932.
8. H. C. Zhou, J. R. Long and O. M. Yaghi, *Chem. Rev.*, 2012, **112**, 673-674.
9. J. Lee, O. K. Farha, J. Roberts, K. A. Scheidt, S. T. Nguyen and J. T. Hupp, *Chem. Soc. Rev.*, 2009, **38**, 1450-1459.
10. W. G. Lu, Z. W. Wei, Z. Y. Gu, T. F. Liu, J. Park, J. Park, J. Tian, M. W. Zhang, Q. Zhang, T. Gentle, M. Bosch and H. C. Zhou, *Chem. Soc. Rev.*, 2014, **43**, 5561-5593.
11. H. C. Zhou and S. Kitagawa, *Chem. Soc. Rev.*, 2014, **43**, 5415-5418.
12. H. Li, M. Eddaoudi, M. O'Keeffe and O. M. Yaghi, *Nature*, 1999, **402**, 276-279.
13. M. Eddaoudi, J. Kim, N. Rosi, D. Vodak, J. Wachter, M. O'Keeffe and O. M. Yaghi, *Science*, 2002, **295**, 469-472.
14. T. M. O. Popp and O. M. Yaghi, *Acc. Chem. Res.*, 2017, **50**, 532-534.
15. A. Helal, Z. H. Yamani, K. E. Cordova and O. M. Yaghi, *Natl. Sci. Rev.*, 2017, **4**, 296-298.
16. H. Furukawa, U. Muller and O. M. Yaghi, *Angew. Chem. Int. Ed.*, 2015, **54**, 3417-3430.
17. M. A. Meyers, J. McKittrick and P. Y. Chen, *Science*, 2013, **339**, 773-779.
18. A. Kirchon, L. Feng, H. F. Drake, E. A. Joseph and H. C. Zhou, *Chem. Soc. Rev.*, 2018, **47**, 8611-8638.
19. H. X. Deng, C. J. Doonan, H. Furukawa, R. B. Ferreira, J. Towne, C. B. Knobler, B. Wang and O. M. Yaghi, *Science*, 2010, **327**, 846-850.
20. Y. B. Zhang, H. Furukawa, N. Ko, W. X. Nie, H. J. Park, S. Okajima, K. E. Cordova, H. X. Deng, J. Kim and O. M. Yaghi, *J. Am. Chem. Soc.*, 2015, **137**, 2641-2650.

21. K. M. Choi, K. Na, G. A. Somorjai and O. M. Yaghi, *J. Am. Chem. Soc.*, 2015, **137**, 7810-7816.
22. Z. Y. Dong, Y. Z. S. Sun, J. Chu, X. Z. Zhang and H. X. Deng, *J. Am. Chem. Soc.*, 2017, **139**, 14209-14216.
23. Q. C. Xia, Z. J. Li, C. X. Tan, Y. Liu, W. Gong and Y. Cui, *J. Am. Chem. Soc.*, 2017, **139**, 8259-8266.
24. C. X. Tan, X. Han, Z. J. Li, Y. Liu and Y. Cui, *J. Am. Chem. Soc.*, 2018, **140**, 16229-16236.
25. Y. J. Sun, L. X. Sun, D. W. Feng and H. C. Zhou, *Angew. Chem. Int. Ed.*, 2016, **55**, 6471-6475.
26. K. Koh, A. G. Wong-Foy and A. J. Matzger, *Angew. Chem. Int. Ed.*, 2008, **47**, 677-680.
27. L. J. Liu, K. Konstas, M. R. Hill and S. G. Telfer, *J. Am. Chem. Soc.*, 2013, **135**, 17731-17734.
28. H. Furukawa, N. Ko, Y. B. Go, N. Aratani, S. B. Choi, E. Choi, A. O. Yazaydin, R. Q. Snurr, M. O'Keeffe, J. Kim and O. M. Yaghi, *Science*, 2010, **329**, 424-428.
29. C. C. Liang, Z. L. Shi, C. T. He, J. Tang, H. D. Zhou, H. L. Zhou, Y. Lee and Y. B. Zhang, *J. Am. Chem. Soc.*, 2017, **139**, 13300-13303.
30. Q. G. Zhai, X. H. Bu, X. Zhao, D. S. Li and P. Y. Feng, *Acc. Chem. Res.*, 2017, **50**, 407-417.
31. S. T. Zheng, J. J. Bu, T. Wu, C. T. Chou, P. Y. Feng and X. H. Bu, *Angew. Chem. Int. Ed.*, 2011, **50**, 8858-8862.
32. X. Zhao, X. H. Bu, Q. G. Zhai, H. Tran and P. Y. Feng, *J. Am. Chem. Soc.*, 2015, **137**, 1396-1399.
33. J. J. Yang, Y. B. Zhang, Q. Liu, C. A. Trickett, E. Gutierrez-Puebla, M. A. Monge, H. J. Cong, A. Aldossary, H. X. Deng and O. M. Yaghi, *J. Am. Chem. Soc.*, 2017, **139**, 6448-6455.
34. S. Yuan, J. S. Qin, L. F. Zou, Y. P. Chen, X. Wang, Q. Zhang and H. C. Zhou, *J. Am. Chem. Soc.*, 2016, **138**, 6636-6642.
35. G. Zhang, M. Tsujimoto, D. Packwood, N. T. Duong, Y. Nishiyama, K. Kadota, S. Kitagawa and S. Horike, *J. Am. Chem. Soc.*, 2018, **140**, 2602-2609.
36. H. Jiang, J. T. Jia, A. Shkurenko, Z. J. Chen, K. Adil, Y. Belmabkhout, L. J. Weselinski, A. H. Assen, D. X. Xue, M. O'Keeffe and M. Eddaoudi, *J. Am. Chem. Soc.*, 2018, **140**, 8858-8867.
37. Y. Wang, L. Feng, W. Fan, K. Y. Wang, X. Wang, X. Wang, K. Zhang, X. Zhang, F. Dai, D. Sun and H. C. Zhou, *J. Am. Chem. Soc.*, 2019, **141**, 6967-6975.
38. O. Karagiaridi, W. Bury, J. E. Mondloch, J. T. Hupp and O. K. Farha, *Angew. Chem. Int. Ed.*, 2014, **53**, 4530-4540.
39. S. J. Garibay and S. M. Cohen, *Chem. Comm.*, 2010, **46**, 7700-7702.
40. S. M. Cohen, *Chem. Rev.*, 2012, **112**, 970-1000.
41. K. K. Tanabe and S. M. Cohen, *Chem. Soc. Rev.*, 2011, **40**, 498-519.
42. Z. Q. Wang and S. M. Cohen, *Chem. Soc. Rev.*, 2009, **38**, 1315-1329.
43. M. Kim, J. F. Cahill, H. H. Fei, K. A. Prather and S. M. Cohen, *J. Am. Chem. Soc.*, 2012, **134**, 18082-18088.
44. C. Liu, T. Y. Luo, E. S. Feura, C. Zhang and N. L. Rosi, *J. Am. Chem. Soc.*, 2015, **137**, 10508-10511.
45. C. Liu, C. J. Zeng, T. Y. Luo, A. D. Merg, R. C. Jin and N. L. Rosi, *J. Am. Chem. Soc.*, 2016, **138**, 12045-12048.
46. K. C. Jayachandrababu, D. S. Sholl and S. Nair, *J. Am. Chem. Soc.*, 2017, **139**, 5906-5915.
47. J. A. Boissonnault, A. G. Wong-Foy and A. J. Matzger, *J. Am. Chem. Soc.*, 2017, **139**, 14841-14844.
48. U. Fluch, V. Paneta, D. Primetzhofer and S. Ott, *Chem. Comm.*, 2017, **53**, 6516-6519.
49. S. Yuan, Y.-P. Chen, J.-S. Qin, W. Lu, L. Zou, Q. Zhang, X. Wang, X. Sun and H.-C. Zhou, *J. Am. Chem. Soc.*, 2016, **138**, 8912-8919.
50. S. Yuan, W. Lu, Y.-P. Chen, Q. Zhang, T.-F. Liu, D. Feng, X. Wang, J. Qin and H.-C. Zhou, *J. Am. Chem. Soc.*, 2015, **137**, 3177-3180.
51. C. X. Chen, Z. W. Wei, J. J. Jiang, S. P. Zheng, H. P. Wang, Q. F. Qu, C. C. Cao, D. Fenske and C. Y. Su, *J. Am. Chem. Soc.*, 2017, **139**, 6034-6037.
52. X. Zhang, B. L. Frey, Y. S. Chen and J. Zhang, *J. Am. Chem. Soc.*, 2018, **140**, 7710-7715.
53. J. D. Pang, S. Yuan, J. S. Qin, M. Y. Wu, C. T. Lollar, J. L. Li, N. Huang, B. Li, P. Zhang and H. C. Zhou, *J. Am. Chem. Soc.*, 2018, **140**, 12328-12332.
54. S. Yuan, J. S. Qin, J. L. Li, L. Huang, L. Feng, Y. Fang, C. Lollar, J. D. Pang, L. L. Zhang, D. Sun, A. Alsalme, T. Cagin and H. C. Zhou, *Nat. Comm.*, 2018, **9**, 808.
55. L. J. Wang, H. X. Deng, H. Furukawa, F. Gandara, K. E. Cordova, D. Peri and O. M. Yaghi, *Inorg. Chem.*, 2014, **53**, 5881-5883.
56. Q. Liu, H. J. Cong and H. X. Deng, *J. Am. Chem. Soc.*, 2016, **138**, 13822-13825.
57. Q. G. Zhai, X. H. Bu, C. Y. Mao, X. Zhao and P. Y. Feng, *J. Am. Chem. Soc.*, 2016, **138**, 2524-2527.

58. A. Schoedel, A. J. Cairns, Y. Belmabkhout, L. Wojtas, M. Mohamed, Z. J. Zhang, D. M. Proserpio, M. Eddaoudi and M. J. Zaworotko, *Angew. Chem. Int. Ed.*, 2013, **52**, 2902-2905.
59. B. B. Tu, Q. Q. Pang, H. S. Xu, X. M. Li, Y. L. Wang, Z. Ma, L. H. Weng and Q. W. Li, *J. Am. Chem. Soc.*, 2017, **139**, 7998-8007.
60. Y. X. Tan, X. Yang, B. B. Li and D. Q. Yuan, *Chem. Comm.*, 2016, **52**, 13671-13674.
61. P. F. Muldoon, C. Liu, C. C. Miller, S. B. Koby, A. G. Jarvi, T. Y. Luo, S. Saxena, M. O'Keeffe and N. L. Rosi, *J. Am. Chem. Soc.*, 2018, **140**, 6194-6198.
62. Q. Liu, Y. Song, Y. Ma, Y. Zhou, H. Cong, C. Wang, J. Wu, G. Hu, M. O'Keeffe and H. Deng, *J. Am. Chem. Soc.*, 2018.
63. B. B. Tu, L. Diestel, Z. L. Shi, W. R. L. N. Bandara, Y. Chen, W. M. Lin, Y. B. Zhang, S. G. Telfer and Q. W. Li, *Angew. Chem. Int. Ed.*, 2019, **58**, 5348-5353.
64. S. Yuan, J. S. Qin, H. Q. Xu, J. Su, D. Rossi, Y. P. Chen, L. L. Zhang, C. Lollar, Q. Wang, H. L. Jiang, D. H. Son, H. Y. Xu, Z. H. Huang, X. D. Zou and H. C. Zhou, *ACS Cent. Sci.*, 2018, **4**, 105-111.
65. S. Das, H. Kim and K. Kim, *J. Am. Chem. Soc.*, 2009, **131**, 3814-3815.
66. M. S. Denny, L. R. Parent, J. P. Patterson, S. K. Meena, H. Pham, P. Abellan, Q. M. Ramasse, F. Paesani, N. C. Gianneschi and S. M. Cohen, *J. Am. Chem. Soc.*, 2018, **140**, 1348-1357.
67. S. Yuan, Y. P. Chen, J. S. Qin, W. G. Lu, X. Wang, Q. Zhang, M. Bosch, T. F. Liu, X. Z. Lian and H. C. Zhou, *Angew. Chem. Int. Ed.*, 2015, **54**, 14696-14700.
68. H. G. T. Nguyen, N. M. Schweitzer, C. Y. Chang, T. L. Drake, M. C. So, P. C. Stair, O. K. Farha, J. T. Hupp and S. T. Nguyen, *ACS Catal.*, 2014, **4**, 2496-2500.
69. Z. Y. Li, A. W. Peters, V. Bernales, M. A. Ortuno, N. M. Schweitzer, M. R. DeStefano, L. C. Gallington, A. E. Platero-Prats, K. W. Chapman, C. J. Cramer, L. Gagliardi, J. T. Hupp and O. K. Farha, *ACS Cent. Sci.*, 2017, **3**, 31-38.
70. Z. Y. Li, A. W. Peters, A. E. Platero-Prats, J. Liu, C. W. Kung, H. Noh, M. R. DeStefano, N. M. Schweitzer, K. W. Chapman, J. T. Hupp and O. K. Farha, *J. Am. Chem. Soc.*, 2017, **139**, 15251-15258.
71. S. Yuan, P. Zhang, L. L. Zhang, A. T. Garcia-Esparza, D. Sokaras, J. S. Qin, L. Feng, G. S. Day, W. M. Chen, H. F. Drake, P. Elumalai, S. T. Madrahimov, D. F. Sun and H. C. Zhou, *J. Am. Chem. Soc.*, 2018, **140**, 10814-10819.
72. S. Yuan, J. S. Qin, J. Su, B. Li, J. L. Li, W. M. Chen, H. F. Drake, P. Zhang, D. Q. Yuan, J. L. Zuo and H. C. Zhou, *Angew. Chem. Int. Ed.*, 2018, **57**, 12578-12583.
73. S. Furukawa, K. Hirai, K. Nakagawa, Y. Takashima, R. Matsuda, T. Tsuruoka, M. Kondo, R. Haruki, D. Tanaka, H. Sakamoto, S. Shimomura, O. Sakata and S. Kitagawa, *Angew. Chem. Int. Ed.*, 2009, **48**, 1766-1770.
74. K. Hirai, S. Furukawa, M. Kondo, H. Uehara, O. Sakata and S. Kitagawa, *Angew. Chem. Int. Ed.*, 2011, **50**, 8057-8061.
75. K. Koh, A. G. Wong-Foy and A. J. Matzger, *Chem. Comm.*, 2009, 6162-6164.
76. T. Li, J. E. Sullivan and N. L. Rosi, *J. Am. Chem. Soc.*, 2013, **135**, 9984-9987.
77. S. Choi, T. Kim, H. Ji, H. J. Lee and M. Oh, *J. Am. Chem. Soc.*, 2016, **138**, 14434-14440.
78. J. Yang, F. J. Zhang, H. Y. Lu, X. Hong, H. L. Jiang, Y. Wu and Y. D. Li, *Angew. Chem. Int. Ed.*, 2015, **54**, 10889-10893.
79. D. Saliba, M. Ammar, M. Rammal, M. Al-Ghoul and M. Hmadeh, *J. Am. Chem. Soc.*, 2018, **140**, 1812-1823.
80. G. W. Zhan and H. C. Zeng, *Nat. Comm.*, 2018, **9**.
81. L. Feng, J.-L. Li, G. S. Day, X.-L. Lv and H.-C. Zhou, *Chem*, 2019, **5,** 1265-1274.
82. Y. F. Gu, Y. N. Wu, L. C. Li, W. Chen, F. T. Li and S. Kitagawa, *Angew. Chem. Int. Ed.*, 2017, **56**, 15658-15662.
83. X. Y. Yang, S. Yuan, L. F. Zou, H. Drake, Y. M. Zhang, J. S. Qin, A. Alsalme and H. C. Zhou, *Angew. Chem. Int. Ed.*, 2018, **57**, 3927-3932.
84. L. Feng, S. Yuan, J. L. Li, K. Y. Wang, G. S. Day, P. Zhang, Y. Wang and H. C. Zhou, *ACS Cent. Sci.*, 2018, **4**, 1719-1726.
85. S. A. Yuan, L. F. Zou, J. S. Qin, J. L. Li, L. Huang, L. A. Feng, X. A. Wang, M. Bosch, A. Alsalme, T. Cagin and H. C. Zhou, *Nat. Comm.*, 2017, **8**, 15356.
86. L. Feng, S. Yuan, J.-S. Qin, Y. Wang, A. Kirchon, D. Qiu, L. Cheng, S. T. Madrahimov and H.-C. Zhou, *Matter*, 2019, DOI: 10.1016/j.matt.2019.02.002.
87. L. Feng, S. Yuan, L. L. Zhang, K. Tan, J. L. Li, A. Kirchon, L. M. Liu, P. Zhang, Y. Han, Y. J. Chabal and H. C. Zhou, *J. Am. Chem. Soc.*, 2018, **140**, 2363-2372.

88. B. Bueken, N. Van Velthoven, A. Krajnc, S. Smolders, F. Taulelle, C. Mellot-Draznieks, G. Mali, T. D. Bennett and D. De Vos, *Chem. Mater.*, 2017, **29**, 10478-10486.
89. V. Guillerm, H. Xu, J. Albalad, I. Imaz and D. Maspoch, *J. Am. Chem. Soc.*, 2018, **140**, 15022-15030.
90. T. D. Bennett, T. K. Todorova, E. F. Baxter, D. G. Reid, C. Gervais, B. Bueken, B. Van de Voorde, D. De Vos, D. A. Keen and C. Mellot-Draznieks, *Phys. Chem. Chem. Phys.*, 2016, **18**, 2192-2201.
91. C. Atzori, G. C. Shearer, L. Maschio, B. Civalleri, F. Bonino, C. Lamberti, S. Svelle, K. P. Lillerud and S. Bordiga, *The Journal of Physical Chemistry C*, 2017, **121**, 9312-9324.
92. X. Q. Kong, H. X. Deng, F. Y. Yan, J. Kim, J. A. Swisher, B. Smit, O. M. Yaghi and J. A. Reimer, *Science*, 2013, **341**, 882-885.
93. A. M. Katzenmeyer, J. Canivet, G. Holland, D. Farrusseng and A. Centrone, *Angew. Chem. Int. Ed.*, 2014, **53**, 2852-2856.
94. L. J. Liu and S. G. Telfer, *J. Am. Chem. Soc.*, 2015, **137**, 3901-3909.
95. L. J. Liu, T. Y. Zhou and S. G. Telfer, *J. Am. Chem. Soc.*, 2017, **139**, 13936-13943.
96. J. Cornelio, T. Y. Zhou, A. Alkas and S. G. Telfer, *J. Am. Chem. Soc.*, 2018, **140**, 15470-15476.
97. M. Pan, Y. X. Zhu, K. Wu, L. Chen, Y. J. Hou, S. Y. Yin, H. P. Wang, Y. N. Fan and C. Y. Su, *Angew. Chem. Int. Ed.*, 2017, **56**, 14582-14586.
98. A. P. Cote, A. I. Benin, N. W. Ockwig, M. O'Keeffe, A. J. Matzger and O. M. Yaghi, *Science*, 2005, **310**, 1166-1170.
99. Y. B. Zhang, J. Su, H. Furukawa, Y. F. Yun, F. Gandara, A. Duong, X. D. Zou and O. M. Yaghi, *J. Am. Chem. Soc.*, 2013, **135**, 16336-16339.
100. T. Q. Ma, E. A. Kapustin, S. X. Yin, L. Liang, Z. Y. Zhou, J. Niu, L. H. Li, Y. Y. Wang, J. Su, J. Li, X. G. Wang, W. D. Wang, W. Wang, J. L. Sun and O. M. Yaghi, *Science*, 2018, **361**, 48-52.
101. F. Haase, E. Troschke, G. Savasci, T. Banerjee, V. Duppel, S. Dorfler, M. M. J. Grundei, A. M. Burow, C. Ochsenfeld, S. Kaskel and B. V. Lotsch, *Nat. Commun.*, 2018, **9**, 2600.
102. A. Nagai, Z. Q. Guo, X. Feng, S. B. Jin, X. Chen, X. S. Ding and D. L. Jiang, *Nat. Commun.*, 2011, **2**, 536.
103. Z. F. Pang, S. Q. Xu, T. Y. Zhou, R. R. Liang, T. G. Zhan and X. Zhao, *J. Am. Chem. Soc.*, 2016, **138**, 4710-4713.
104. Y. F. Zeng, R. Y. Zou, Z. Luo, H. C. Zhang, X. Yao, X. Ma, R. Q. Zou and Y. L. Zhao, *J. Am. Chem. Soc.*, 2015, **137**, 1020-1023.
105. X. Chen, M. Addicoat, E. Q. Jin, H. Xu, T. Hayashi, F. Xu, N. Huang, S. Irle and D. L. Jiang, *Sci. Rep.*, 2015, **5**, 14650.
106. H. Q. Li, Q. Y. Qi, X. Zhao, G. S. Li, X. Chen, H. J. Zhang and J. B. Lin, *Polym. Chem.*, 2018, **9**, 4288-4293.
107. N. Huang, L. P. Zhai, D. E. Coupry, M. A. Addicoat, K. Okushita, K. Nishimura, T. Heine and D. L. Jiang, *Nat. Commun.*, 2016, **7**, 12325.
108. N. Huang, R. Krishna and D. L. Jiang, *J. Am. Chem. Soc.*, 2015, **137**, 7079-7082.
109. Y. J. Yang, M. Faheem, L. L. Wang, Q. H. Meng, H. Y. Sha, N. Yang, Y. Yuan and G. S. Zhu, *ACS Cent. Sci.*, 2018, **4**, 748-754.
110. W. Ji, L. L. Xiao, Y. H. Ling, C. Ching, M. Matsumoto, R. P. Bisbey, D. E. Helbling and W. R. Dichtel, *J. Am. Chem. Soc.*, 2018, **140**, 12677-12681.
111. H. Xu, X. Chen, J. Gao, J. B. Lin, M. Addicoat, S. Irle and D. L. Jiang, *Chem. Comm.*, 2014, **50**, 1292-1294.
112. H. Xu, J. Gao and D. L. Jiang, *Nat. Chem.*, 2015, **7**, 905-912.
113. J. Zhang, X. Han, X. W. Wu, Y. Liu and Y. Cui, *J. Am. Chem. Soc.*, 2017, **139**, 8277-8285.
114. L. Chen, K. Furukawa, J. Gao, A. Nagai, T. Nakamura, Y. P. Dong and D. L. Jiang, *J. Am. Chem. Soc.*, 2014, **136**, 9806-9809.
115. A. M. Rice, E. A. Dolgopolova, B. J. Yarbrough, G. A. Leith, C. R. Martin, K. S. Stephenson, R. A. Heugh, A. J. Brandt, D. A. Chen, S. G. Karakalos, M. D. Smith, K. B. Hatzell, P. J. Pellechia, S. Garashchuk and N. B. Shustova, *Angew. Chem. Int. Ed.*, 2018, **57**, 11310-11315.
116. F. Xu, H. Xu, X. Chen, D. C. Wu, Y. Wu, H. Liu, C. Gu, R. W. Fu and D. L. Jiang, *Angew. Chem. Int. Ed.*, 2015, **54**, 6814-6818.
117. M. A. Khayum, V. Vijayakumar, S. Karak, S. Kandambeth, M. Bhadra, K. Suresh, N. Acharambath, S. Kurungot and R. Banerjee, *ACS Appl. Mater. Inter.*, 2018, **10**, 28139-28146.
118. L. Ascherl, T. Sick, J. T. Margraf, S. H. Lapidus, M. Calik, C. Hettstedt, K. Karaghiosoff, M. Doblinger, T. Clark, K. W. Chapman, F. Auras and T. Bein, *Nat. Chem.*, 2016, **8**, 310-316.
119. F. Auras, L. Ascherl, A. H. Haldmioun, J. T. Margraf, F. C. Hanusch, S. Reuter, D. Bessinger, M. Doblinger, C. Hettstedt, K. Karaghiosoff, S.

Herbert, P. Knochel, T. Clark and T. Bein, *J. Am. Chem. Soc.*, 2016, **138**, 16703-16710.
120. X. Chen, M. Addicoat, S. Irle, A. Nagai and D. L. Jiang, *J. Am. Chem. Soc.*, 2013, **135**, 546-549.
121. L. M. Salonen, D. D. Medina, E. Carbo-Argibay, M. G. Goesten, L. Mafra, N. Guldris, J. M. Rotter, D. G. Stroppa and C. Rodriguez-Abreu, *Chem. Comm.*, 2016, **52**, 7986-7989.
122. X. Chen, M. Addicoat, E. Q. Jin, L. P. Zhai, H. Xu, N. Huang, Z. Q. Guo, L. L. Liu, S. Irle and D. L. Jiang, *J. Am. Chem. Soc.*, 2015, **137**, 3241-3247.
123. R. A. Maia, F. L. Oliveira, M. Nazarkovsky and P. M. Esteves, *Cryst. Growth Des.*, 2018, **18**, 5682-5689.
124. X. W. Wu, X. Han, Y. H. Liu, Y. Liu and Y. Cui, *J. Am. Chem. Soc.*, 2018, **140**, 16124-16133.
125. X. Han, J. Zhang, J. J. Huang, X. W. Wu, D. Q. Yuan, Y. Liu and Y. Cui, *Nat. Commun.*, 2018, **9,** 1294.
126. N. Keller, M. Calik, D. Sharapa, H. R. Soni, P. M. Zehetmaier, S. Rager, F. Auras, A. C. Jakowetz, A. Gorling, T. Clark and T. Bein, *J. Am. Chem. Soc.*, 2018, **140**, 16544-16552.
127. P. Albacete, J. I. Martinez, X. Li, A. Lopez-Moreno, S. Mena-Hernando, A. E. Platero-Prats, C. Montoro, K. P. Loh, E. M. Perez and F. Zamora, *J. Am. Chem. Soc.*, 2018, **140**, 12922-12929.
128. X. Guan, Y. Ma, H. Li, Y. Yusran, M. Xue, Q. Fang, Y. Yan, V. Valtchev and S. Qiu, *J. Am. Chem. Soc.*, 2018, **140**, 4494-4498.
129. T. Q. Ma, J. Li, J. Niu, L. Zhang, A. S. Etman, C. Lin, D. E. Shi, P. H. Chen, L. H. Li, X. Du, J. L. Sun and W. Wang, *J. Am. Chem. Soc.*, 2018, **140**, 6763-6766.
130. Y. Z. Liu, Y. H. Ma, Y. B. Zhao, X. X. Sun, F. Gandara, H. Furukawa, Z. Liu, H. Y. Zhu, C. H. Zhu, K. Suenaga, P. Oleynikov, A. S. Alshammari, X. Zhang, O. Terasaki and O. M. Yaghi, *Science*, 2016, **351**, 365-369.
131. Y. Z. Liu, Y. H. Ma, J. J. Yang, C. S. Diercks, N. Tamura, F. Y. Jin and O. M. Yaghi, *J. Am. Chem. Soc.*, 2018, **140**, 16015-16019.
132. S. Kandambeth, V. Venkatesh, D. B. Shinde, S. Kumari, A. Halder, S. Verma and R. Banerjee, *Nat. Commun.*, 2015, **6**, 6786.
133. A. Halder, S. Kandambeth, B. P. Biswal, G. Kaur, N. C. Roy, M. Addicoat, J. K. Salunke, S. Banerjee, K. Vanka, T. Heine, S. Verma and R. Banerjee, *Angew. Chem. Int. Ed.*, 2016, **55**, 7806-7810.
134. B. Gole, V. Stepanenko, S. Rager, M. Grune, D. D. Medina, T. Bein, F. Wurthner and F. Beuerle, *Angew. Chem. Int. Ed.*, 2018, **57**, 846-850.
135. G. Das, T. Skorjanc, S. K. Sharma, F. Gandara, M. Lusi, D. S. S. Rao, S. Vimala, S. K. Prasad, J. Raya, D. S. Han, R. Jagannathan, J. C. Olsen and A. Trabolsi, *J. Am. Chem. Soc.*, 2017, **139**, 9558-9565.
136. S. Kim, C. Park, M. Lee, I. Song, J. Kim, M. Lee, J. Jung, Y. Kim, H. Lim and H. C. Choi, *Adv. Funct. Mater.*, 2017, **27**, 1700925.
137. P. Pachfule, S. Kandmabeth, A. Mallick and R. Banerjee, *Chem. Comm.*, 2015, **51**, 11717-11720.
138. J. Tan, S. Namuangruk, W. F. Kong, N. Kungwan, J. Guo and C. C. Wang, *Angew. Chem. Int. Ed.*, 2016, **55**, 13979-13984.
139. J. H. Sun, A. Klechikov, C. Moise, M. Prodana, M. Enachescu and A. V. Talyzin, *Angew. Chem. Int. Ed.*, 2018, **57**, 1034-1038.
140. B. Q. Li, S. Y. Zhang, L. Kong, H. J. Peng and Q. Zhang, *Adv. Mater.*, 2018, **30**.
141. B. Olenyuk, J. A. Whiteford, A. Fechtenkotter and P. J. Stang, *Nature*, 1999, **398**, 796-799.
142. N. Takeda, K. Umemoto, K. Yamaguchi and M. Fujita, *Nature*, 1999, **398**, 794.
143. M. Eddaoudi, J. Kim, J. B. Wachter, H. K. Chae, M. O'Keeffe and O. M. Yaghi, *J. Am. Chem. Soc.*, 2001, **123**, 4368-4369.
144. K. E. Jelfs, E. G. B. Eden, J. L. Culshaw, S. Shakespeare, E. O. Pyzer-Knapp, H. P. G. Thompson, J. Bacsa, G. M. Day, D. J. Adams and A. I. Cooper, *J. Am. Chem. Soc.*, 2013, **135**, 9307-9310.
145. S. Klotzbach and F. Beuerle, *Angew. Chem. Int. Ed.*, 2015, **54**, 10356-10360.
146. K. E. Jelfs, X. F. Wu, M. Schmidtmann, J. T. A. Jones, J. E. Warren, D. J. Adams and A. I. Cooper, *Angew. Chem. Int. Ed.*, 2011, **50**, 10653-10656.
147. Q. F. Sun, J. Iwasa, D. Ogawa, Y. Ishido, S. Sato, T. Ozeki, Y. Sei, K. Yamaguchi and M. Fujita, *Science*, 2010, **328**, 1144-1147.
148. W. M. Bloch and G. H. Clever, *Chem. Comm.*, 2017, **53**, 8506-8516.
149. F. Beuerle and B. Gole, *Angew. Chem. Int. Ed*, 2018, **57**, 4850-4878.
150. S. Hiraoka, Y. Kubota and M. Fujita, *Chem. Comm.*, 2000, 1509-1510.

151. K. Kumazawa, K. Biradha, T. Kusukawa, T. Okano and M. Fujita, *Angew. Chem. Int. Ed.*, 2003, **42**, 3909-3913.
152. M. Yamashina, T. Yuki, Y. Sei, M. Akita and M. Yoshizawa, *Chem.-Eur. J.*, 2015, **21**, 4200-4204.
153. Q. F. Sun, S. Sato and M. Fujita, *Angew. Chem. Int. Ed.*, 2014, **53**, 13510-13513.
154. W. M. Bloch, Y. Abe, J. J. Holstein, C. M. Wandtke, B. Dittrich and G. H. Clever, *J. Am. Chem. Soc.*, 2016, **138**, 13750-13755.
155. W. M. Bloch, J. J. Holstein, W. Hiller and G. H. Clever, *Angew. Chem. Int. Ed.*, 2017, **56**, 8285-8289.
156. J. R. Li and H. C. Zhou, *Nat. Chem.*, 2010, **2**, 893-898.
157. A. M. Johnson and R. J. Hooley, *Inorg. Chem.*, 2011, **50**, 4671-4673.
158. D. Preston, J. E. Barnsley, K. C. Gordon and J. D. Crowley, *J. Am. Chem. Soc.*, 2016, **138**, 10578-10585.
159. Y. R. Zheng, Z. G. Zhao, M. Wang, K. Ghosh, J. B. Pollock, T. R. Cook and P. J. Stang, *J. Am. Chem. Soc.*, 2010, **132**, 16873-16882.
160. S. J. Rowan, S. J. Cantrill, G. R. L. Cousins, J. K. M. Sanders and J. F. Stoddart, *Angew. Chem. Int. Ed.*, 2002, **41**, 898-952.
161. F. B. L. Cougnon and J. K. M. Sanders, *Acc. Chem. Res.*, 2012, **45**, 2211-2221.
162. K. Acharyya, S. Mukherjee and P. S. Mukherjee, *J. Am. Chem. Soc.*, 2013, **135**, 554-557.
163. K. Acharyya and P. S. Mukherjee, *Chem.-Eur. J.*, 2014, **20**, 1646-1657.
164. K. Acharyya and P. S. Mukherjee, *Chem. Comm.*, 2015, **51**, 4241-4244.
165. S. Jiang, J. T. A. Jones, T. Hasell, C. E. Blythe, D. J. Adams, A. Trewin and A. I. Cooper, *Nat. Commun.*, 2011, **2**, 207.
166. G. H. Zhu, Y. Liu, L. Flores, Z. R. Lee, C. W. Jones, D. A. Dixon, D. S. Sholl and R. P. Lively, *Chem. Mater.*, 2018, **30**, 262-272.
167. M. Fujita, *Acc. Chem. Res.*, 1999, **32**, 53-61.
168. C. S. Wood, T. K. Ronson, A. M. Belenguer, J. J. Holstein and J. R. Nitschke, *Nat. Chem.*, 2015, **7**, 354-358.
169. D. M. Engelhard, S. Freye, K. Grohe, M. John and G. H. Clever, *Angew. Chem. Int. Ed.*, 2012, **51**, 4747-4750.
170. S. L. Huang, Y. J. Lin, Z. H. Li and G. X. Jin, *Angew. Chem. Int. Ed.*, 2014, **53**, 11218-11222.
171. M. Fujita, N. Fujita, K. Ogura and K. Yamaguchi, *Nature*, 1999, **400**, 52-55.
172. M. Fukuda, R. Sekiya and R. Kuroda, *Angew. Chem. Int. Ed.*, 2008, **47**, 706-710.
173. S. Freye, J. Hey, A. Torras-Galan, D. Stalke, R. Herbst-Irmer, M. John and G. H. Clever, *Angew. Chem. Int. Ed.*, 2012, **51**, 2191-2194.
174. S. Freye, R. Michel, D. Stalke, M. Pawliczek, H. Frauendorf and G. H. Clever, *J. Am. Chem. Soc.*, 2013, **135**, 8476-8479.
175. R. M. Zhu, J. Lubben, B. Dittrich and G. H. Clever, *Angew. Chem. Int. Ed.*, 2015, **54**, 2796-2800.
176. W. M. Bloch, J. J. Holstein, B. Dittrich, W. Hiller and G. H. Clever, *Angew. Chem. Int. Ed.*, 2018, **57**, 5534-5538.
177. T. Hasell, X. F. Wu, J. T. A. Jones, J. Bacsa, A. Steiner, T. Mitra, A. Trewin, D. J. Adams and A. I. Cooper, *Nat. Chem.*, 2010, **2**, 750-755.
178. G. Zhang, O. Presly, F. White, I. M. Oppel and M. Mastalerz, *Angew. Chem. Int. Ed.*, 2014, **53**, 5126-5130.
179. R. Greenaway, V. Santolini, M. J. Bennison, B. M. Alston, C. J. Pugh, M. A. Little, M. Miklitz, E. G. B. Eden-Rumps, R. Clowes, A. Shakil, H. J. Cuthbertson, H. Armstrong, M. E. Briggs, K. E. Jelfs and A. I. Cooper, *Nat. Commun.*, 2018, **9**, 2849.
180. W. Wei, W. L. Li, X. Z. Wang and J. Y. He, *Cryst. Growth Des.*, 2013, **13**, 3843-3846.
181. D. Luo, X. P. Zhou and D. Li, *Angew. Chem. Int. Ed.*, 2015, **54**, 6190-6195.
182. Z. Niu, S. Fang, X. Liu, J. G. Ma, S. Q. Ma and P. Cheng, *J. Am. Chem. Soc.*, 2015, **137**, 14873-14876.
183. A. Carne-Sanchez, G. A. Craig, P. Larpent, T. Hirose, M. Higuchi, S. Kitagawa, K. Matsuda, K. Urayama and S. Furukawa, *Nat. Commun.*, 2018, **9**, 2506.
184. P. Sutar, V. M. Suresh, K. Jayaramulu, A. Hazra and T. K. Maji, *Nat. Commun.*, 2018, **9**, 3587.
185. A. V. Zhukhovitskiy, M. Z. Zhong, E. G. Keeler, V. K. Michaelis, J. E. P. Sun, M. J. A. Hore, D. J. Pochan, R. G. Griffin, A. P. Willard and J. A. Johnson, *Nat. Chem.*, 2016, **8**, 33-41.
186. Y. F. Wang, Y. W. Gu, E. G. Keeler, J. V. Park, R. G. Griffin and J. A. Johnson, *Angew. Chem. Int. Ed.*, 2017, **56**, 188-192.
187. A. V. Zhukhovitskiy, J. Zhao, M. J. Zhong, E. G. Keeler, E. A. Alt, P. Teichen, R. G. Griffin, M. J. A. Hore, A. P. Willard and J. A. Johnson, *Macromolecules*, 2016, **49**, 6896-6902.

188. Y. W. Gu, E. A. Alt, H. Wang, X. P. Li, A. P. Willard and J. A. Johnson, *Nature*, 2018, **560**, 65-69.
189. J. T. A. Jones, T. Hasell, X. F. Wu, J. Bacsa, K. E. Jelfs, M. Schmidtmann, S. Y. Chong, D. J. Adams, A. Trewin, F. Schiffman, F. Cora, B. Slater, A. Steiner, G. M. Day and A. I. Cooper, *Nature*, 2011, **474**, 367-371.
190. T. Hasell, S. Y. Chong, M. Schmidtmann, D. J. Adams and A. I. Cooper, *Angew. Chem. Int. Ed.*, 2012, **51**, 7154-7157.
191. M. J. Bojdys, M. E. Briggs, J. T. A. Jones, D. J. Adams, S. Y. Chong, M. Schmidtmann and A. I. Cooper, *J. Am. Chem. Soc.*, 2011, **133**, 16566-16571.
192. A. G. Slater, M. A. Little, A. Pulido, S. Y. Chong, D. Holden, L. Chen, C. Morgan, X. Wu, G. Cheng, R. Clowes, M. E. Briggs, T. Hasell, K. E. Jelfs, G. M. Day and A. I. Cooper, *Nat. Chem.*, 2017, **9**, 17-25.
193. S. Jiang, Y. Du, M. Marcello, E. W. Corcoran, D. C. Calabro, S. Y. Chong, L. J. Chen, R. Clowes, T. Hasell and A. I. Cooper, *Angew. Chem. Int. Ed.*, 2018, **57**, 11228-11232.
194. J.-R. Li, D. J. Timmons and H.-C. Zhou, *J. Am. Chem. Soc.*, 2009, **131**, 6368-6369.
195. L. Zhang, L. Xiang, C. Hang, W. L. Liu, W. Huang and Y. C. Pan, *Angew. Chem. Int. Ed.*, 2017, **56**, 7787-7791.
196. Y. Kim, J. Koo, I. C. Hwang, R. D. Mukhopadhyay, S. Hong, J. Yoo, A. A. Dar, I. Kim, D. Moon, T. J. Shin, Y. H. Ko and K. Kim, *J. Am. Chem. Soc.*, 2018, **140**, 14547-14551.
197. G. Lal, M. Derakhshandeh, F. Akhtar, D. Spasyuk, M. Trifkovic and G. K. H. Shimizu, *J. Am. Chem. Soc.*, 2019, **141**, 1045-1053.
198. S. I. Swamy, J. Bacsa, J. T. Jones, K. C. Stylianou, A. Steiner, L. K. Ritchie, T. Hasell, J. A. Gould, A. Laybourn, Y. Z. Khimyak, D. J. Adams, M. J. Rosseinsky and A. I. Cooper, *J. Am. Chem. Soc.*, 2010, **132**, 12773-12775.
199. Y. Inokuma, T. Arai and M. Fujita, *Nat. Chem.*, 2010, **2**, 780-783.
200. Y. Inokuma, N. Kojima, T. Arai and M. Fujita, *J. Am. Chem. Soc.*, 2011, **133**, 19691-19693.
201. L. P. Cao, P. P. Wang, X. R. Miao, Y. H. Dong, H. Wang, H. H. Duan, Y. Yu, X. P. Li and P. J. Stang, *J. Am. Chem. Soc.*, 2018, **140**, 7005-7011.
202. Z. Wang, H. Ma, T. L. Zhai, G. Cheng, Q. Xu, J. M. Liu, J. K. Yang, Q. M. Zhang, Q. P. Zhang, Y. S. Zheng, B. Tan and C. Zhang, *Adv. Sci.*, 2018, **5**, 1800141.
203. A. Dutta, K. Koh, A. G. Wong-Foy and A. J. Matzger, *Angew. Chem. Int. Ed.*, 2015, **54**, 3983-3987.
204. H. L. Nguyen, F. Gandara, H. Furukawa, T. L. H. Doan, K. E. Cordova and O. M. Yaghi, *J. Am. Chem. Soc.*, 2016, **138**, 4330-4333.
205. F. M. Zhang, J. L. Sheng, Z. D. Yang, X. J. Sun, H. L. Tang, M. Lu, H. Dong, F. C. Shen, J. Liu and Y. Q. Lan, *Angew. Chem. Int. Ed.*, 2018, **57**, 12106-12110.
206. Y. W. Peng, M. T. Zhao, B. Chen, Z. C. Zhang, Y. Huang, F. N. Dai, Z. C. Lai, X. Y. Cui, C. L. Tan and H. Zhang, *Adv. Mater.*, 2018, **30**, 1705454.
207. D. Sun, S. Jang, S. J. Yim, L. Ye and D. P. Kim, *Adv. Funct. Mater.*, 2018, **28**, 1707110.

This review is expected to provide a library of multi-component hierarchically porous compounds, which shall guide the state-of-art design of future porous materials with unprecedent tunability, synergism and precision.